How nematode sperm crawl

Dean Bottino[1,*], Alexander Mogilner[2], Tom Roberts[3], Murray Stewart[4] and George Oster[1,‡]

[1]Department of Molecular and Cellular Biology, University of California, Berkeley, CA 94720-3112, USA
[2]Department of Mathematics, University of California, Davis, CA 95616, USA
[3]Department of Biological Science, Florida State University, Tallahassee, FL 32306-3050, USA
[4]MRC Laboratory of Molecular Biology, Hills Road, Cambridge CB2 2QH, England
*Present address: Physiome Sciences, 150 College Road West, Princeton, NJ 08540-6608
‡Author for correspondence (e-mail: goster@nature.berkeley.edu)

Accepted 12 October 2001
Journal of Cell Science 115, 367-384 (2002) © The Company of Biologists Ltd

Summary

Sperm of the nematode, *Ascaris suum*, crawl using lamellipodial protrusion, adhesion and retraction, a process analogous to the amoeboid motility of other eukaryotic cells. However, rather than employing an actin cytoskeleton to generate locomotion, nematode sperm use the major sperm protein (MSP). Moreover, nematode sperm lack detectable molecular motors or the battery of actin-binding proteins that characterize actin-based motility. The Ascaris system provides a simple 'stripped down' version of a crawling cell in which to examine the basic mechanism of cell locomotion independently of other cellular functions that involve the cytoskeleton. Here we present a mechanochemical analysis of crawling in Ascaris sperm. We construct a finite element model wherein (a) localized filament polymerization and bundling generate the force for lamellipodial extension and (b) energy stored in the gel formed from the filament bundles at the leading edge is subsequently used to produce the contraction that pulls the rear of the cell forward. The model reproduces the major features of crawling sperm and provides a framework in which amoeboid cell motility can be analyzed. Although the model refers primarily to the locomotion of nematode sperm, it has important implications for the mechanics of actin-based cell motility.

Movies available on-line.

Key words: Cell motility, Major sperm protein, Nematode sperm cell, Amoeboid movements, Cytoskeleton

Introduction

Crawling cells move by using the actin cytoskeleton to power a simple mechanical cycle whereby the leading edge protrudes and adheres to the substratum. The cell body is then pulled forward in a process generally called retraction (Abercrombie, 1980; Roberts and Stewart, 2000). Delineating the mechanochemical events that drive this cycle has proven elusive because of the large number of proteins involved in cell locomotion and the intricacy of the intracellular control system. Moreover, the involvement of actin in a range of other cellular functions, such as endo- and exocytosis, trafficking and maintenance of cell shape, has frustrated the interpretation of many experiments. Therefore, we have focused on a simple and specialized cell: the sperm of a nematode, *Ascaris suum*. In these cells, the locomotion machinery is dramatically simplified, thereby providing a unique and powerful perspective for evaluating the molecular mechanism of cell crawling (Italiano et al., 2001; Roberts and Stewart, 2000).

Nematode sperm exhibit the same cycle of protrusion, adhesion and retraction as actin-driven amoeboid cells. This shared motile behavior suggests that both types of cell employ analogous molecular mechanisms to generate locomotion (Roberts and Stewart, 2000). However, nematode sperm lack the actin machinery typically associated with amoeboid cell motility; instead, their movement is powered by a cytoskeleton built from major sperm protein (MSP) filaments*. MSP is a highly basic 14.5 kDa polypeptide that polymerizes in a hierarchical fashion (Roberts and Stewart, 1995; Roberts and Stewart, 1997). The protein forms symmetrical dimers in solution that polymerize into helical subfilaments, which wind together in pairs to form larger filaments. Because of their unique structure, MSP filaments can spontaneously assemble into higher-order assemblies using the same interaction interfaces employed to assemble subfilaments into filaments (King et al., 1994b; Stewart et al., 1994). Thus, in contrast to actin, MSP polymerization and bundling does not require a broad spectrum of accessory proteins. Moreover, within subfilaments, the polymer has no overall structural polarity (Bullock et al., 1998). This lack of structural polarity implies that motor proteins are unlikely to play a major role in MSP-mediated cell motility, as motors require substrate polarity to define the direction of their movement.

The MSP cytoskeleton of *Ascaris* sperm is organized into 20-30 branched, densely packed filament meshworks, called fiber complexes, that span the lamellipod from the leading edge to the base where they join the cell body (Fig. 1). Filaments extend out laterally from adjacent fiber complexes and intertwine so that the entire cytoskeleton forms a thixotropic (shear thinning) gel that operates mechanically as

*Recently, it has been shown that MSP is involved in cellular signaling as well as motility (Miller et al., 2001).

a unit*. Filaments are assembled and bundled into fiber complexes along the leading edge and disassembled at the base of the lamellipod. Thus, as the cell crawls forward, the cytoskeleton treadmills continuously rearward through the lamellipod (Italiano et al., 2001; Roberts and Stewart, 2000). The rate of centripetal cytoskeletal flow matches that of locomotion. Thus, elongation of the fiber complexes is coupled to protrusion of the leading edge, whereas retraction of the cell body is associated with disassembly of the cytoskeleton at the opposite end of the lamellipod. These observations form the basis of a proposed 'push-pull' mechanism for crawling movement, whereby protrusion and retraction are linked reciprocally to the assembly status of the MSP machinery (Italiano et al., 1999; Roberts and Stewart, 2000).

The MSP motility system offers powerful advantages for modeling the mechanochemistry of cell crawling. Unlike actin, which is used for a variety of cellular activities, the MSP machinery is dedicated solely to locomotion and appears to require only a small number of additional proteins to function. This molecular simplicity greatly facilitates analysis of movement and interpretation of experimental data. In addition, the forces for protrusion and retraction in nematode sperm are generated at opposite ends of a highly organized cytoskeleton in an organelle-free lamellipod. Cytoskeletal dynamics are not obscured by other cellular activities and can be observed directly by light microscopy. Moreover, these processes have been uncoupled by experimental manipulation of the cell and can be reconstituted both in vivo and in vitro. Thus, sperm offer a simple and specialized experimental system for investigating how cells crawl and one in which the components of the locomotion machinery are reduced to a minimum (Italiano et al., 2001; Roberts and Stewart, 2000).

In this manuscript we describe a detailed physical model that accounts for the major aspects of nematode sperm motility and that provides a conceptual framework for evaluating the contribution of different aspects of cytoskeleton dynamics and assembly to locomotion. The layout of the paper is as follows. In the following section we describe a 2D mechanical model for the *Ascaris* lamellipod. In the third section, we discuss the various possible physical and chemical rationalizations for the assumptions underlying the model and the experimental observations that impact upon each mechanism. In the fourth section, we compare the results of model simulations with the observed motile behavior of sperm and the results of selected experimental manipulations of motility. Finally, in Section 5, we discuss the unified view that the model brings to the integrative aspects of lamellipodial motility.

Description of the model

In this section we describe a computational model developed on the basis of a finite element representation of the MSP cytoskeletal gel system. As the details are quite complicated, mathematical particulars of the model are given in the Appendices. The physical basis for assumptions underlying the model is discussed in the next section.

The model we present is a quantitative biophysical formulation of the 'push-pull' hypothesis (Roberts and Stewart, 2000). The physical property of the MSP filaments that underlies the model's behavior is their propensity to spontaneously associate laterally into higher order filament

*The gel is thixotropic because the bonds/crosslinks between filaments are labile and can break and reform under a deforming load.

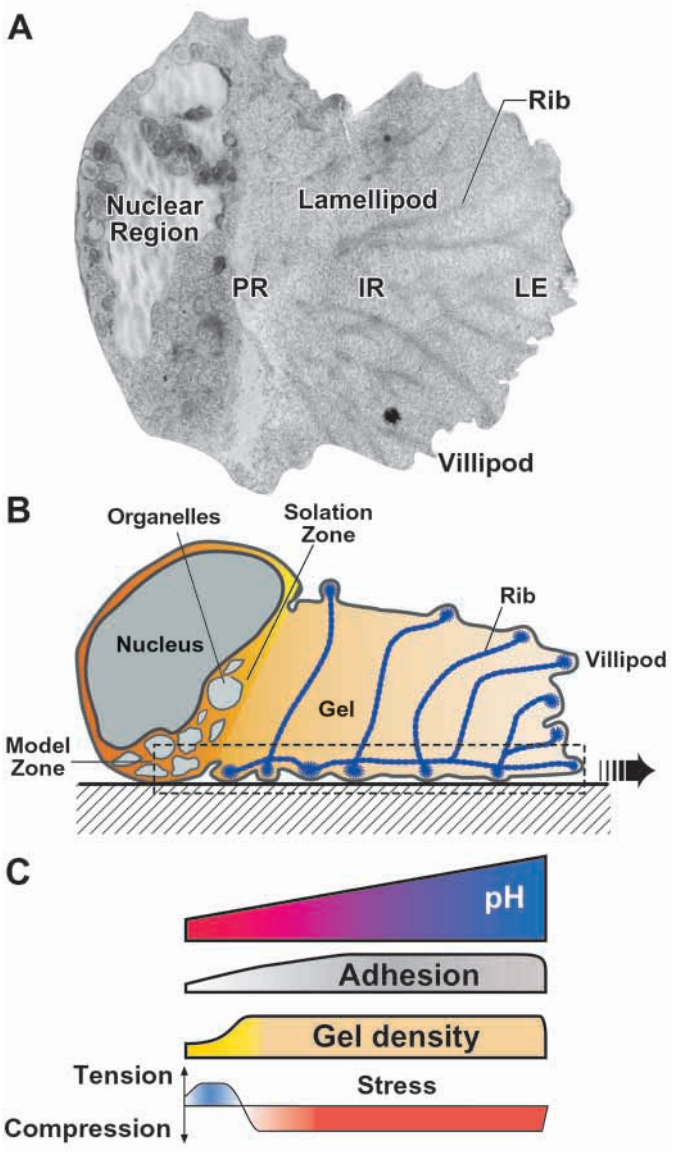

Fig. 1. (A) Top view of a crawling *Ascaris* sperm. The lamellipod can be divided into three major regions: (LE), the leading edge where polymerization and gel condensation into macrofibers and ribs takes place. In *Ascaris*, but not in other nematode sperm, hyper-complexed branched MSP 'ribs' are prominent and originate in protuberances called villipodia. (PR) the perinuclear region where the MSP gel solates and generates a contractile stress. (IR) the intermediate region between the LE and PR where the gel density is nearly constant. The proximal-to-distal pH gradient affects the polymerization and depolymerization rates at the LE and in the PR. (B) Schematic diagram showing the *Ascaris* sperm lamellipod in cross section. The ventral-fiber complexes branch dorsally. The MSP gel forms at the leading edge and is connected mechanically to the substratum through the membrane. As the cell moves forwards, the gel remains stationary with respect to the substratum, eventually entering the perinuclear region where it solates and contracts. (C) The graphs show how the pH, adhesion, gel density and the elastic stress vary with position in the lamellipod.

structures and networks as a result of their unusual macromolecular structure (King et al., 1994b; Stewart et al., 1994). This association produces a fibrous gel that crosslinks via a number of self-association sites on the surface of the MSP filaments. The polymerization and bundling of MSP can be modulated by altering cellular pH (Italiano et al., 2001; Italiano et al., 1999; Roberts et al., 1998). A range of observations lead to the conclusion that assembly generates a protrusive force (Italiano et al., 1996), whereas disassembly generates a contractile force (Italiano et al., 1999), a process suggested by several authors for actin-based systems (Mogilner and Oster, 1996b; Oster, 1988; Oster and Perelson, 1988; Taylor et al., 1979). The model we present here shows how the mechanical balance of forces explains the major features of the protrusion-adhesion-retraction cycle that propels the cell. We also propose a plausible physical basis for each of the component forces.

In *Ascaris* sperm, cell polarity coincides with a proximal-distal pH gradient of ~0.2 pH units (King et al., 1994a). Experimental manipulation of this gradient alters MSP cytoskeletal organization and dynamics, suggesting that intracellular pH contributes to the regulation of the motility machinery (Italiano et al., 1999; King et al., 1992). The origin of the pH gradient is not known but probably results from the mitochondria that are excluded from the MSP gel and so cluster in the cell body at the base of the lamellipod. A range of experimental studies (Roberts and Stewart, 2000) have demonstrated that polymerization and gel formation occurs in the more basic environment at the leading edge of the lamellipod, whereas solation and depolymerization take place predominantly in the more acidic environment of the proximal region near the cell body.

The general idea of the model is as follows. MSP polymerizes at the leading edge to form filaments that spontaneously assemble into bundles that form a fibrous gel. This bundling process pushes the cell front forwards. We propose that gel assembly also stores elastic energy in the form of a tensile stress in the gel. As the cell moves forward, the MSP gel moves proximally towards the cell body where the environment is more acidic until solation of the gel is triggered. The solation process releases the elastic energy in the gel generating a contractile stress. We further propose that adhesion of the lamellipodium to the substratum also decreases in the acidic environment at the rear of the cell. Thus, the gel contraction accompanying solation pulls the cell body forwards rather than pulling the leading edge back.

The remainder of this section is devoted to describing how the finite element model implements these forces. The Appendix explains the model in greater detail and formulates it as mathematical equations. To discuss the various physicochemical processes taking place, we divide the lamellipodium of crawling sperm into three general regions, shown in Fig. 1A: (1) the leading edge (LE); (2) the intermediate region (IR) comprising the bulk of the lamellipodium; and (3) the solation, or perinuclear, region (PR).

The finite element model

The complexity of the interactions and the geometry preclude direct mathematical analysis; therefore, we use a finite element model to investigate the dynamic consequences of the physical forces described above*. The bulk of the MSP gel is located at the ventral surface of the lamellipod; the dorsal volume does not contribute significantly to locomotion. Moreover, while there is probably significant water flow in the 3D body of the cell, close to the ventral boundary, there is little fluid flow. Therefore, a 2D model is sufficient to represent many aspects of the mechanics of crawling. In a subsequent study, we will extend the model to three dimensions and incorporate fluid flow explicitly into the model.

The basic physics of the MSP gel model can be captured in a simple 1D model that represents an anterior-posterior transect, as shown in Fig. 2A. The 2D version that is the basis for the finite element model is given in the Appendix. Consider a strip of cytogel with unit cross sectional area extending from the leading edge to the cell rear. Denote by u(x) the displacement of a material point from its initial position. For

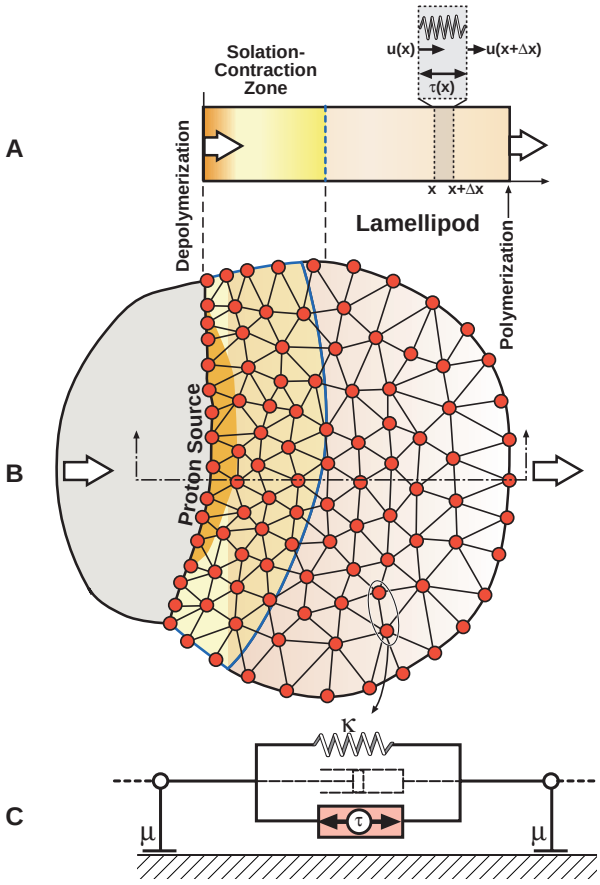

Fig. 2. (A) The continuum model of a 1D cytogel strip representing the lamellipod (see Appendix). (B) The finite element model of the lamellipod. The lamellipod is triangulated so that each node represents a mass of cytoskeleton contained in the surrounding (Voronoi) polygon. (C) Detail of a finite element consisting of an elastic element in parallel with a tensile element. The dashpot with damping coefficient μ connected to the substratum accounts for the viscous dissipation associated with making and breaking attachments as well as the dissipation associated with cytoskeleton-fluid friction.

*A good elementary introduction to the finite element method can be found in Strang (Strang, 1986). Here we will present the model using a more heuristic approach.

small displacements, the strain is just the gradient in the displacement $\varepsilon(x)=\partial u(x)/\partial x$ [or, in 2D: $\varepsilon(x)=\frac{1}{2}(\nabla u + \nabla u^T)$]. For small strains, the stress in a small element of an elastic body, $\sigma(x)$, at position x is related to the strain, $\varepsilon(x)$, by Hooke's law (Landau and Lifshitz, 1995):

$$\sigma(x) = Y \cdot \varepsilon(x) \quad (1)$$

where Y is the elastic modulus (Young's modulus) of the material.

We propose that the MSP gel differs from a simple elastic material in several ways, the most important being the ability to store elastic energy as it coalesces into higher-order macromolecular assemblies such as fiber complexes. We shall discuss the physical basis for this 'bundling stress' below. The mechanical effect of bundling is to add a tensile stress term to equation (1):

$$\sigma(\mathbf{x}) = \underbrace{Y\varepsilon(\mathbf{x})}_{\substack{\text{Elastic}\\ \text{Stress}}} - \underbrace{\tau(\mathbf{x})}_{\substack{\text{Tensile}\\ \text{Stress}}} \quad (2)$$

Here $\tau(x)$ represents the combined dilating effects of the gel osmotic pressure (this includes the gel entropic motions and the counterion pressure) and the 'bundling' stress discussed below. Finally, an additional body force must be added to (2) owing to the adhesive forces holding the lamellipod to the substratum. As the cell moves forward, these forces manifest themselves as a frictional drag proportional to the speed of locomotion:

$$\mu(\mathbf{x})\frac{\partial \mathbf{u}(x,t)}{\partial t} = \text{drag force on the cell at position x} \quad (3)$$

where $\mu(x)$ is the drag coefficient that characterizes the effective resistance to motion. μ includes the making and breaking of adhesions of the lamellipod to the substratum as well as the viscous resistance of the cytoplasm to the forces exerted by the cytoskeleton. Using (3), the force balance on a small element of the cytogel strip is (Landau and Lifshitz, 1995):

$$\underbrace{\mu\frac{\partial u}{\partial t}}_{\text{Drag Force}} = \underbrace{\frac{\partial}{\partial x}\left(Y\frac{\partial u}{\partial x} - \tau\right)}_{\text{Elastic + Swelling Forces}} \quad \text{In 2-D: } \left[\mu\frac{\partial \mathbf{u}}{\partial t} = \nabla\cdot\sigma(\mathbf{u})\right] \quad (4)$$

The MSP gel polymerizes at the right hand (leading) boundary of the strip and depolymerizes at the left (rear) boundary. At these boundaries a load-velocity relationship must be specified; the boundary conditions and the solutions to equation (4) are given in the Appendix.

Figure 2B shows the tessellation of the 2D lamellipod into triangular elements. Each branch of the tessellation represents the mechanical element shown in Figure 2C. It consists of a spring with elastic modulus, κ, in parallel with an extensional force generator that applies a tension to the element. This represents the tensile stress, τ, in equation (2). The retarding force attributable to the substratum adhesions is represented by the sliding friction element between the element node and the substratum. There is also internal dissipation in the gel owing to the relative motion between the fibers and the solvent. This is represented in Figure 2C as an additional dashpot, shown by a dashed line, in parallel with the spring and force generator. In our simulations we have incorporated this internal dissipation into the sliding friction dashpot to the substratum. The equations of the finite element model are constructed by collecting together all of the force balances at each node of the tessellation, each equation being the finite version of equation (4); for example, for node i:

$$\underbrace{\mu\frac{\partial x_i}{\partial t}}_{\text{Drag Force}} = \sum_{j=1}^{n}\left(\underbrace{\kappa(x_j - x_i)}_{\text{Spring force}} - \underbrace{\tau_{ij}}_{\substack{\text{Tensile}\\ \text{force}}}\right), \quad i = 1...N \quad (5)$$

Here n is the number of branches incident on node i, and N is the total number of nodes. Nodes in the intermediate region of the lamellipodium are governed by equations of the form (5). Elements at the leading edge and in the perinuclear region must be handled differently. The Appendix lays out the complete computational algorithm driving the model.

Elements at the leading edge

As the tessellated cell moves forward, new nodes must be introduced at the leading edge to represent polymerization and bundling of the MSP gel. Since actual polymerization takes place within a few tens of nanometers of the leading edge membrane (Italiano et al., 1996), we cannot represent this process explicitly in a model for the whole lamellipod. Therefore, we represent the composite process of protrusion and gel condensation as follows.

As a result of MSP polymerization and bundling, the leading edge advances by the extension of bulbous protrusions called villipodia. These protuberances do not touch the substratum as they expand, but eventually they settle into contact and establish adhesions. Thus the leading node of the model does not have a viscous element (dashpot) connecting to the substratum, and the leading branch consists only of the elastic and tensile elements in parallel. This implies that a leading branch is stress free: the tensile force that represents the (negative) gradient in the free energy of crosslinking balances the elastic force.

Each leading edge branch extends by lengthening at a velocity determined by the rate of MSP polymerization and bundling. These two processes are generated by factors in the leading edge of the lamellipod membrane (Italiano et al., 1996). When a branch reaches twice its original length, a node is inserted at the midpoint along with a viscous element to the substratum so that a new LE and IR branch is formed.

Elements in the solation region

Each node surrogates for a volume of MSP gel represented by the Voronoi polygon surrounding the node (Bottino, 2001)*. In order to conserve mass, the number of nodes must be conserved†. Therefore, as new nodes are introduced at the leading edge, nodes must be removed at the cell rear at the same average rate. As the gel solates in the acidic environment near the cell body, the elastic energy stored in each branch is released to pull the cell forwards. This is accomplished as follows. The most posterior nodes are anchored to the cell body

*Voronoi polygons partition space into territories, each of which consists of the points closer to one particular node than to any others (Okabe, 2000). The finite elements used in the model derive from this particular way of partitioning the cytogel.

†Strictly speaking, since the cell is 3D, the ventral area can vary if its height changes, without altering the total volume of the cell. However, in our 2D model, we assume that the cell height is constant and so the lamellipodial area is equivalent to the cell volume.

and are permanent. When a node approaches the cell rear closer than a threshold distance, that node is removed along with its dashpot to the substratum. Solation is modeled by removing the tensile elements in parallel with the remaining springs, which have been held in tension. This allows the springs in series to contract to their original rest length. In this way the free energy of crosslinking that was supplied to the system at the front end is released to pull up the cell rear. This algorithm combines both the solation-contraction process and the ultimate depolymerization of the MSP gel to dimers, which are then recycled to the leading edge.

Protrusion and solation rates are modulated by pH

An essential feature of the model is that MSP assembly and disassembly are separated spatially. Although clearly both are influenced by pH, it is likely that protrusion is controlled primarily by factors present in the membrane at the leading edge of the lamellipod provided that the pH is above about 6.8. Under these conditions, a membrane protein (VP) acts in conjunction with at least two soluble cytoplasmic proteins (SF) to facilitate local MSP polymerization (Roberts et al., 1998). This process can be inhibited when the pH is lowered: addition of pH 6.35 – 6.7 external acetate buffer stops MSP polymerization and bundling at the leading edge of the lamellipod (Italiano et al., 1999). However, under these conditions MSP unbundling and depolymerization still continues at the cell body and generates a force that places the cytoskeleton under tension. The pH at the site of cytoskeletal disassembly is lower than that at the leading edge (King et al., 1994a), and so depolymerization and unbundling could be initiated when the pH falls below a critical value near the cell body. Although the precise role played by pH in either assembly or disassembly has yet to be established, the pH is clearly a good marker for these processes. Therefore, we have used pH as a convenient surrogate to model the way in which the balance between MSP assembly and disassembly changes in the lamellipod between its leading edge and the cell body. In our calculations, we compute the proton distribution throughout the lamellipod at each time step. We assume that the proton source is located at the boundary between the lamellipod and the cell body. Protons also leak out from the lamellipod at the boundaries. Since the diffusion rate of protons is very rapid, we can assume that the concentration profile is always at its steady state for a given boundary profile. At each time step, the concentration is updated according to the changed boundary shape, and the polymerization and depolymerization rates are computed accordingly (see Appendix).

Forces in the lamellipod

In this section we discuss the physicochemical basis for the forces introduced in the finite element model and present the relevant experimental data.

Protrusion

Lamellipodial protrusion has been reconstituted in vitro in cell-free extracts of *Ascaris* sperm. Vesicles derived from the leading-edge membrane induce the localized assembly of MSP filaments that arrange into cylindrical meshworks, called fibers, that push the vesicle forward as they elongate (Italiano et al., 1996). These vesicles contain a phosphorylated form of VP that recruits SF to the membrane where it nucleates polymerization. Thus, MSP dimers are ‘activated’ by VP and SF at the leading edge, whereupon they become polymerization competent and quickly polymerize into filaments. Unlike actin, MSP does not bind to nucleotides directly (Bullock et al., 1996; Italiano et al., 1996). ATP hydrolysis is required for phosphorylation of VP, but the precise role of ATP in MSP polymerization is unclear. The filaments formed in the vicinity of the membrane assemble laterally into higher order filament complexes (Sepsenwol et al., 1989). In *Ascaris*, fiber complexes are visible by light microscopy as ‘rope-like’ ribs that project from the leading edge to the cell body, forming a branched tree-like pattern. However, these large fiber complexes are prominent in *Ascaris* compared to sperm from other nematode species (e.g. *C. elegans*), indicating that their size is probably not crucial to generating locomotion. Therefore, we do not include them as a separate level of gelation in the model.

The concentration of SF and the activation of VP, rather than that of MSP itself, appear to be limiting for polymerization (Italiano et al., 1996; Roberts et al., 1998). The mechanism by which these proteins are localized and controlled is not known; in the Appendix, we present several theoretical possibilities. In the model, polymerization depends only on local pH near the boundary of the lamellipod. The equations governing the polymerization process are given in the Appendix.

To model protrusion at the leading edge we must provide a load-velocity relationship that prescribes the force generated at the leading edge by the formation of the MSP gel. The proposal that polymerization drives the extension of lamellipodia in actin-based systems has a long history going back to the classic work of Abercrombie (Abercrombie, 1980). Recently, Mogilner and Oster examined the physics of force generation by a semi-stiff polymerizing actin filament – the elastic polymerization ratchet model (Mogilner and Oster, 1996a; Mogilner and Oster, 1996b). However, MSP filaments appear to be somewhat more flexible than actin, and so the polymerization ratchet mechanism may not be as effective in generating a protrusive force in nematode sperm. However, the process of bundling filaments into higher order macromolecular assemblies can also contribute to the protrusive force; the calculation that supports this assertion is discussed in the Appendix. In the MSP model, we introduce a pressure at the cell boundary that pushes the cell periphery outwards in the direction normal to the local edge tangent. This pressure arises from the assembly and bundling of MSP filaments into a gel as follows.

Newly polymerized MSP filaments are created stress free and are relatively flexible (i.e. they have a short persistence length). Because of the unusual way in which MSP filaments are generated (i.e. by wrapping two helical subfilaments around one another), they have a series of mutual interaction sites arranged on their surface so that they are able to form bundles spontaneously without the specific bundling proteins actin requires (Stewart et al., 1994). This property is seen most dramatically in the macrofibers formed when MSP is assembled in vitro (King et al., 1994b) but is also probably responsible for the various higher order aggregates of MSP filaments observed in vivo. Consequently, the distribution of these mutual interaction sites on the surface of MSP filaments means that filaments that diffuse into contact with one another will adhere and assemble into higher order filament bundles

spontaneously*. This assembly process forces the filaments within a higher-order aggregate to assume an end-to-end distance that is larger than it was in solution. That is, the enthalpic part of the free energy of assembly dominates the entropy loss accompanying lateral association, so that filaments are held in a 'stretched' configuration. Thus, bundles of MSP filaments contain the stored elastic energy of their constituent filaments (analogous to a pre-stressed concrete beam) and are stiffer. These bundles of MSP form a thixotropic gel-like cytoskeleton within the lamellipod. The cytoskeletal gel is a fibrous material, so that when filaments bundle laterally they generate a protrusive force longitudinally (Poisson expansion). This may help extrude the leading edge into the characteristic protuberances (villipodia) that characterize the motile sperm (Sepsenwol et al., 1989).

Near the leading edge membrane, a number of associated processes take place. As MSP molecules interact with one another, both during filament polymerization and macrofiber assembly, counterions are released and the local gel osmotic pressure decreases. Moreover, fiber-associated 'vicinal' water associated with both filament polymerization and lateral association is released (Pollack, 2001). The sensitivity of the polymerization and bundling of MSP to pressure may be due to this water release and/or to weakening of lateral hydrophobic interactions between filaments (Roberts et al., 1998). It is difficult to assess the quantitative effect of these processes, but they probably also contribute to lamellipodial protrusion and villipodia formation.

Adhesion

To move forward the lamellipod must adhere to the substratum. Examination of crawling sperm by interference reflection microscopy has revealed that the adhesive sites are located primarily in the lamellipod, with few if any in the cell body. In these cells, close contacts form between the lamellipod membrane and the glass substratum. The pattern of these contacts varies; in some cells almost the entire underside of the lamellipod is attached to the glass, whereas others exhibit a series of discrete contact sites. In all cases, the contacts form just behind the leading edge, remain stationary as the cell progresses, and release when the lamellipod-cell body junction passes over the contact site (T. Rodriguez and T. Roberts, unpublished observations). Thus, the pattern of adhesion appears nearly constant from the leading edge to the transition region in the perinuclear region, that is the strength of adhesion appears to be nearly a 'step' function. The adhesion gradient determines the direction of crawling by preventing the leading edge from being pulled back by gel contraction; instead the cell rear is pulled forward. For the purposes of the model, we assume that the adhesion strength is piecewise linear: strong at high values of pH, weak at low values of pH, with a linear transition at some intermediate value of pH (Fig. 6). The Appendix discusses the adhesion and release processes in more detail.

Retraction

The third component of the crawling cycle is retraction – the contraction that pulls up the cell rear. In actin-based systems, the mechanism that generates this contraction is myosin-driven contraction of the lamellipodial actin (Lin et al., 1996; Svitkina et al., 1997; Oliver et al., 1999; Verkhovsky et al., 1999)†. Because MSP filaments lack the structural polarity required for motor proteins to function, it is unlikely that the mechanism of retraction in nematode sperm is based on molecular motors. Instead, we propose the following mechanism for retraction. As the MSP gel moves posteriorly (with respect to the leading edge), it encounters a rising proton concentration. The protons compete with the electrostatic crosslinking sites and weaken the hydrophobic interactions as well. The weakening of the cohesive forces in the MSP filaments and bundles allows individual MSP filaments to dissociate from the fiber complexes. As they do so, they attempt to contract entropically to their equilibrium end-to-end length. Because the gel is an entangled meshwork, a contractile stress develops in the gel. Because adhesion is weaker in the rear than in the front of the cell, this contraction pulls the back of the cell forward.

This picture is supported by the following observations on the MSP-associated motion of single vesicles. Italiano et al. (Italiano et al., 1996) demonstrated that membrane vesicles reconstituted from motile sperm can nucleate cylindrical MSP 'tails' and propel these vesicles forwards, similar to the actin tails growing behind microspheres coated with ActA (Cameron et al., 1999). When these MSP gel tails are exposed to acidic conditions, they shrink. If one end of the tail is attached to the substratum, the vesicle at the other end is pulled towards the attachment point (L. Miao and T. Roberts, unpublished).

An interfacial tension effect probably also contributes to pulling the rear of the cell forward. The density of the MSP filament gel decreases across the gel-sol transition region, which is typically very narrow. Along phase transition boundaries such as this interface, a tangential stress will develop, similar to the interfacial tension at a liquid-vapor interface. This interfacial tension, combined with the stress in the low density region, pulls the cell body forward. The response of *Ascaris* sperm to manipulation of intracellular pH supports the idea that interfacial tension is involved in cell body retraction. For example, treatment of the cells with acetate buffer at pH<6 causes the MSP cytoskeleton to disassemble completely. When the acid is washed out, intracellular pH rebounds, and the cytoskeleton is rebuilt by reconstruction of the fiber complexes along the lamellipod membrane. These newly formed complexes lengthen by assembly at their membrane-associated ends. The opposite ends move rearward through the lamellipod, creating an interface between the proximal boundary of the reforming cytoskeleton and the lamellipod cytoplasm. Retraction of the cell rear does not commence until this interface reaches the cell body, implying that depolymerization of the fiber

*The attraction between like-charged polymers comes about due to two effects. First, multivalent counterions can displace the layered water near the polymer surface and create salt bridges between filaments (Pollack, 2001). A more subtle, but well documented, phenomenon involves counterion condensation and correlated charge fluctuations. Recent discussions can be found in Manning and Ray and others (Manning and Ray, 1998; Stevens, 1999; Stevens, 2001). Also, it is not clear to what extent molecular crowding and associated excluded volume effects may influence this behaviour in the cytoplasm of nematode sperm where protein concentrations are probably of the order of 200-400 mg/ml (Ellis, 2001).

†This is firmly established for nerve growth cones (Lin et al., 1996) and fish keratocytes (Svitkina et al., 1997; Verkhovsky et al., 1999). However, the ability of Dictyostelium mutants lacking myosin II to crawl suggests that this protein is not essential for retraction in all actin-based cells (Knecht and Loomis, 1987).

complexes is necessary for retraction. In some cells, this reassembly is asymmetric within the lamellipod; when the reforming fiber complexes contact one side of the cell body before the other, a turning moment develops that moves the cell towards the direction of contact (Italiano et al., 1999).

Depolymerization

Following solation (i.e. disassembly) of the MSP filament bundles and their subsequent entropic contraction, the MSP gel must be depolymerized so that subunits (probably MSP dimers) can be recycled to the leading edge. Since depolymerization creates a proximal-distal subunit gradient, diffusion is sufficient to accomplish this recycling. It is possible that factors other than pH are involved. For example, there is evidence for an 'MSP depolymerization factor' that could also be involved in regulating the depolymerization rate (J. Italiano and T. Roberts, unpublished). In the model, we assume that the depolymerization takes place quickly in a narrow region at the rear of the lamellipod, adjacent to the cell body. Figure 1C summarizes how the gradients in adhesion, gel density and elastic stress follow the pH gradient.

Comparing the model with observations

In the Appendix, we consider a 'minimal' model consisting of a 1D cytogel strip running along the length of the cell. This model can be explored analytically, and it illustrates how the lamellipod length and migration velocity are regulated to maintain constant values. This regulation comes about from a negative-feedback loop that reduces the rate of protrusion in longer lamellipods and increases the rate of protrusion in shorter ones so that protrusion and retraction are matched, corresponding to the observation of coordinated polymerization and depolymerization in living crawling sperm (Italiano et al., 2001; Roberts and Stewart, 2000).

Of course, the 1D model cannot properly address the issue of lamellipodial shape and area regulation, and so a 2D finite element model is required to reproduce the shapes and rates of locomotion of the *Ascaris* sperm cell. To our knowledge, this is the first mathematical model that simulates locomotion using simple dynamic principles of coordination of protrusion, graded adhesion and retraction. The model combines the mechanics of protrusion and contraction with regulatory biochemical pathways and shows how their coupling generates stable rapid migration. The dynamic behavior of the model can best be appreciated by viewing the QuickTime™ movies that can be downloaded from http://www.CNR.Berkeley.EDU/~bottino/research/wormsperm/. Figs 3-5 show frames from these movies (for movie legends, see http://jcs.biologists.org/supplemental).

The model simulates a broad range of features of sperm motility, which are examined below.

Velocity and shape

The model reproduces observed properties of cell locomotion: a steady-state velocity with a shape (length to width ratio of 1:1 to 3:1) consistent with those observed in crawling sperm (Royal et al., 1995; Sepsenwol et al., 1989; Sepsenwol and Taft, 1990) (Fig. 3) (see Movie 1 at http://jcs.biologists.org/supplemental).

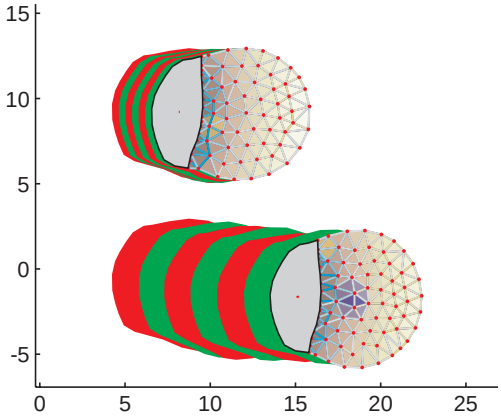

Fig. 3. Frames from the simulation movie showing the progression of the MSP cytoskeleton as the cell moves forward. The same time interval elapses between successive shaded cell 'shadows'. Bottom, simulation of translocation with 'normal' substrate friction. Top, simulation with the cell body friction increased four-fold over the normal run. Note that the cell body moves much more slowly, but the lamellipod shape changes very little.

Shape regulation

To stabilize the length in the 1D model and the area in the 2D model, a pH gradient alone is insufficient. It is necessary to introduce a limiting quantity whose concentration decreases as the lamellipodial size increases. There are several possible candidates, which we discuss below. However, for the model calculations we assumed that the vesicle protein is the limiting quantity. If the amount of vesicle protein is constant, then its concentration in the leading edge dilutes as the lamellipodial area increases. This reduces the MSP polymerization rate. Our simulations show that this is sufficient to regulate the lamellipodial area to a stable average size. Note that the depletion mechanism creates a global negative feedback, whereas pH regulation is local and activating. Thus, a combination of local activation and global inhibition is needed for size regulation.

Persistence

In the absence of external cues, locomotion is persistent: in the computer model, the cell travels many body lengths before it deviates significantly from the initial direction of migration. This is consistent with the observed behavior of crawling cells (Sepsenwol, 1990; Royal et al., 1995).

Robustness

The speed and shape of the lamellipod is not significantly altered by changing the explicit forms of the force-velocity relation at the rear, depolymerization kinetics, pH and density dependencies of the polymerization rate, bundling stress and adhesion strength and elastic stress-strain relation.

Traction forces

We computed the map of traction forces that the lamellipod exerts on the substratum during retrograde flow (Fig. 4). There are significant differences between the pattern of traction forces

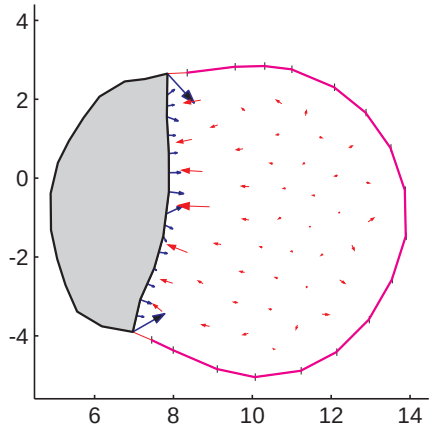

Fig. 4. A vector field plot of forces at nodes computed after the cell moved two body lengths. The interior node forces (red) are applied to the substrate; the cell body interface node forces (blue) are applied throughout the substrate beneath the cell body. The magnitude of the forces are proportional to the lengths of the arrows. The forces applied to the center of the cell body interface are ~100 pN. The total forward translocation force on the cell body is ~1000 pN. The traction forces at the rear of the lamellipod are ≈10 pN per node. Because of the strong substrate adhesion and because there is no gradient in the bundling stress, the traction forces decrease to ~1 pN per node at the leading edge. There is also no noticeable anisotropy in the traction forces.

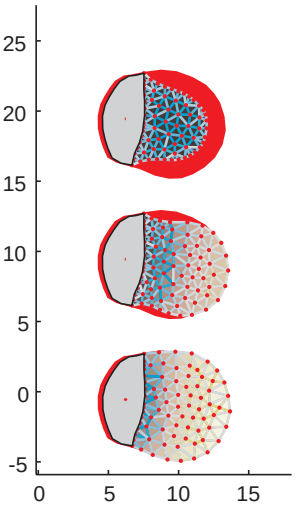

Fig. 5. A study of effects of extracellular pH_{ext} on the simulated cell. In all figures, the red filled region is the original outline of the cell. The final position of the cell in all three cases is shown after the same amount of simulation time has elapsed (~1 sec of real time). Bottom, pH_{ext}=7.6. This is the case of normal motility. At the front, pH reaches the value of >6.15, so that both the storage of elastic energy, cytoskeletal assembly and adhesion are strong at the leading edge. Middle, pH_{ext}=6.75. At this pH motility is impaired. At the front, pH drops to less than 6.15, but both the storage of elastic energy and adhesion are still strong at the leading edge. However, the cytoskeletal assembly is attenuated significantly. The cell body moves forward, but the leading edge is nearly stationary. Top, at pH_{ext}=6.35 this motility ceases. At the front the pH decreases to less than 6.1, so that all of the protrusion-supporting processes – adhesion, storage of elastic energy and cytoskeletal assembly – are inhibited. The contraction of the lamellipod takes place transiently owing to the elastic energy stored prior to the change in extracellular pH. This contraction moves the cell body forward slightly, at the same time pulling the leading edge backward significantly. The adhesion of the cell body is now greater than the adhesion of the lamellipod.

generated by the model from those measured in fish keratocytes and fibroblasts (Dembo et al., 1996; Jacobson et al., 1996; Oliver et al., 1995; Oliver et al., 1999). Gliding sperm develop much smaller traction forces. Also, the distribution of forces in sperm is much more uniform compared with fibroblasts, where there are alignment and 'pinching forces' in the direction of migration in fibroblasts and normal to this direction for keratocytes. This prediction could be evaluated experimentally using elastic films and photobleaching experiments.

Adhesion forces

By increasing the effective adhesion of the cell body to the surface, we simulated the behavior of sperm tethered to the substratum. In these simulations, forward translocation slowed significantly, whereas the rate of retrograde flow in the lamellipod increased. Remarkably, the shape of the lamellipod changed very little. (Fig. 3; Movie 2). These results agree qualitatively with experimental observations (Italiano et al., 1999) and are in striking contrast to actin-based cells where lamellipodial shape and traction force patterns change dramatically in the same situations.

Dependence on pH

Finally, we mimicked the experiment wherein crawling sperm were treated with weak acid at pH 6.35 and pH 6.75, respectively (Italiano et al., 1999) (Fig. 5; Movie 3; Movie 4.) In both the real cell and the model, at pH 6.75, the assembly stops, thus arresting protrusion, whereas adhesion and contraction continue, leading to temporary forward translocation of the cell body. At the same time, the lamellipod begins to shrink. At pH 6.35, also in both the actual cell and the model, both assembly and adhesion are disrupted, whereas contraction continues. The MSP cytoskeleton detaches from the leading edge, flows rearward and is disassembled in the proximal region.

Discussion

We have developed a finite element model of the MSP gel system that generates locomotion in nematode sperm. The model accounts for amoeboid motility by providing a mechanical basis for the processes of lamellipodial protrusion, substrate adhesion and cell body retraction. A central feature of the model is the way in which energy stored in the cytoskeleton gel during protrusion is subsequently released to generate a pulling force on the cell body. Thus, although protrusion and retraction can be separated experimentally (Italiano et al., 1999), in vivo, they rely respectively on the assembly and disassembly dynamics of the MSP cytoskeleton. In addition to providing a physical basis to account for the observed amoeboid motility of nematode sperm, our model also has implications for actin-based cell locomotion.

Nematode sperm motility

Previous studies have demonstrated that the amoeboid motility of nematode sperm closely resembles that seen in many actin-based systems (Roberts and Stewart, 2000). Nematode sperm have a cytoskeleton derived from MSP and lack actin, myosin and tubulin. Nevertheless, their motility shows the same lamellipodial protrusion and cell body retraction seen in actin-based systems and their locomotion also relies on adhesion to the substrate to generate forward motion. A range of

experiments have demonstrated the crucial role played by the vectorial assembly of MSP filaments and their bundling into large aggregates (Roberts and Stewart, 2000). Direct observation of MSP fiber complexes by light microscopy shows that they treadmill, with material being added continuously at the leading edge of the lamellipod and removed near the cell body. In vitro, MSP polymerization and bundling can move membrane vesicles (Italiano et al., 1996), and both this reconstituted motility and cell locomotion show a remarkable sensitivity to pressure (Roberts et al., 1998). The MSP polymerization that takes place at the leading edge of the cell requires both membrane-bound and soluble factors (Roberts et al., 1998). It has been possible to decouple lamellipodial protrusion, membrane-cytoskeletal attachment and cell body retraction by manipulating pH with acetate buffer (Italiano et al., 1999). At pH 6.75 lamellipodial protrusion is inhibited but retraction continues, whereas at pH 6.35 the adhesion of the cytoskeleton to the membrane is broken and the MSP filament system then moves rearward.

Our finite element model for the MSP cytoskeleton gel system reproduces these features of nematode sperm locomotion and gives an unanticipated insight into how retraction is mechanically related to protrusion. At the leading edge of the lamellipod, MSP is polymerized initially to form filaments that bundle to form large fiber complexes that attach to the membrane and, through it, to the substratum. The filaments condense to form the fiber-complex gel by forming a large number of weak crosslinks between filaments. In this configuration, they are held in a more extended conformation than they are in free solution. That is, their persistence length in these aggregates is greater than that in free solution with a consequent loss of entropy, possibly associated with a compensating release of bound water and ions. In this extended configuration, the fiber complexes contain stored elastic energy that, upon release, will provide the contractile stress to pull the cell body forwards. The fiber complexes maintain their shape as they treadmill, suggesting that there is little remodeling of the constituent filaments and filament bundles. Thus, the stored energy is not released until the filaments unbundle and depolymerize at the base of the lamellipod, whereupon the filaments seek to contract to their equilibrium length. Thus elastic energy stored during bundle formation generates tension in the cytoskeleton to pull the cell body forward when the gel solates. Attachment to the substrate is required for both traction and to mechanically separate the forces of protrusion and retraction that are generated at opposite ends of cytoskeleton gel. For this, the lamellipod must adhere more strongly than the cell body, lest the tension generated in the cytoskeleton generated by MSP depolymerization and solation move the lamellipod rearwards rather than the cell body forward.

The ability of our model to simulate both sperm movement and shape indicates that the forces used are sufficient to account for sperm locomotion. The model can also account for the dynamics of cell shape. To our knowledge, there have been no studies that quantitatively address the dynamics of lamellipodial shape. The ‘graded radial extension’ (GRE) model of Lee et al. sheds light on the kinematic principles underlying lamellipodial shape in fish keratocytes (Lee et al., 1993a; Lee et al., 1993b). This model demonstrated that if extension is locally normal to the cell boundary, and if the rate of extension decreases from the center to the sides of the cell, then the 2D steady-state shape of the traveling lamellipod evolves. The model we present here identifies the dynamic principles underlying self-organization of the lamellipod of the nematode sperm and provides a dynamic mechanism for the GRE model. For example, it is likely that lamellipod size regulation is based on a negative-feedback loop involving a limiting factor rather than on the cellular pH gradient alone. Thus, long lamellipods would grow more slowly than short ones and so converge to a roughly constant length. There are a number of plausible molecular mechanisms by which this feedback could be generated. For example, if material such as MSP dimers or SF is being consumed when the fibers form at the leading edge and subsequently liberated near the cell body when MSP depolymerizes, then the concentration of these factors at the leading edge would depend on diffusion and so would be lower the greater the distance of the leading edge from the cell body. Also, the membrane area of the cell would be greater with longer lamellipodia; increasing the membrane area could reduce the concentration of VP per unit area at the leading edge, thus decreasing the supply of polymerization competent subunits and slowing the rate of protrusion. Finally, increasing lamellipodial size may increase the membrane tension, which could decrease the rate of exocytosis (Raucher and Sheetz, 1999a; Raucher and Sheetz, 1999b; Raucher and Sheetz, 2000). If VP is supplied by exocytosis, this would again decrease the polymerization rate.

The model captures the cellular polarization observed in *Ascaris* sperm: construction of the MSP cytoskeleton gel and adhesion to the substratum occur at or near the leading edge, whereas gel solation and de-adhesion take place at the base of the lamellipod. We have discussed the possible molecular basis for these events; however, since the molecular details remain uncertain, we have used the pH gradient present within the cell as a surrogate to model the effect of these processes on motility. It is possible – albeit unlikely – that the pH gradient alone generates cellular polarity directly. For example, the high pH present at the leading edge of the lamellipod could exceed a threshold for operation of the VP-SF nucleation complex that generates MSP assembly at the leading edge, whereas the more acidic environment at the cell body could trigger dissociation of the MSP filament bundles and depolymerize individual filaments. However, it is equally likely that the pH gradient is associated with intervening regulatory proteins that perform the actual work of gelation and solation.

It is admittedly an approximation to use the pH gradient to represent both the spatial separation of MSP assembly from disassembly and adhesion from de-adhesion. However, the finite element model simulates motile behavior of nematode sperm in remarkable detail. This simple model can account for persistence in the direction of locomotion, the maintenance of cell shape, the continuation of cytoskeletal flow when the lamellipod is not in contact with substratum and the behavior of tethered cells. Thus the model encapsulates the primary mechanochemistry of the motile process and can serve as a conceptual framework in which the amoeboid motility of nematode sperm can be understood. The model provides a physical realization of the push-pull model of nematode sperm motility and describes how MSP filament assembly and bundling can generate the forces required for cell locomotion. In a subsequent study, we shall refine the model to include the fluid and solid phases of the MSP gel, which will enable us to

match a large number of additional observations on cytoplasmic flow (manuscript in preparation).

Implications for actin-based cell motility

The general principles of lamellipodial-driven cell locomotion have been established for some time: a cycle of protrusion, graded adhesion and retraction drives translocation (Abercrombie, 1980). However, many details remain elusive. Broadly speaking, there are two fundamental questions that need to be resolved: (1) What is the physical nature and the molecular basis of protrusion, retraction, and adhesion? (2) How are the three processes coordinated to achieve the observed shapes and rates of migrating cells?

Our simulations of the nematode sperm have implications for the mechanism of locomotion of actin-based cells. Although the mechanical principles of motility seem to be remarkably similar for nematode sperm and many actin-based cells, the force-generating mechanisms, biochemical components and regulatory pathways employed to modulate cytoskeletal polymerization and organization are different. The concept that lamellipodial protrusion is driven primarily by localized filament polymerization and self-organization into the network, which was established in nematode sperm (Italiano et al., 1996), is now generally accepted as the basis for protrusion in actin-based systems as well (Borisy and Svitkina, 2000; Theriot, 2000). The molecular mechanisms, and the relative contributions of polymerization and network organization, differ in the actin and MSP machinery. For example, the polymerization ratchet model, proposed to account for protrusion in actin systems, places the physical basis for force generation on subunit addition at the ends of filaments that bend away from the membrane and then spring back (Mogilner and Oster, 1996a; Mogilner and Oster, 1996b). This mechanism also requires that the filaments be arranged into a branching meshwork by the action of nucleating and minus-end-capping proteins such as Arp2/3 (Blanchoin et al., 2000; Pantaloni et al., 2001; Pollard et al., 2000; Pollard et al., 2001). In the MSP system, in which filaments spontaneously aggregate to form higher order arrays, bundling may be the dominate force generating mechanism, although polymerization is also required.

Another difference between actin- and MSP-driven systems is that the force for retraction in sperm involves depolymerization and unbundling, whereas in many actin-based systems retraction appears to be driven by myosin (Lin et al., 1996; Verkhovsky et al., 1999; Verkhovsky et al., 1995). For example, the dynamic contraction model of Verkhovsky et al. suggests that disruption of the actin cytoskeletal gel by depolymerization and dissociation of Arp2/3 complexes weakens actin in the posterior region (Verkhovsky et al., 1999). This allows collapse of the largely isotropic actin network into bi-polar actin-myosin bundles and subsequent sliding contraction. In contrast, the present model demonstrates that solation and depolymerization of the MSP cytoskeleton can, in principle, use energy stored during the formation of the cytoplasmic gel during protrusion to generate a tension that can be used to pull the cell body forward. Thus, the results obtained using nematode sperm suggest that motor proteins may not be the whole story (Bullock et al., 1998; Italiano et al., 1999). It is plausible that, in actin systems, the energy released when filament networks are taken apart could be used to contribute to the forward motion of the cell body, in addition to the actin-myosin sliding mechanism (Mogilner and Oster, 1996b).

In summary, we have constructed a physical model that accounts for the major features of nematode sperm amoeboid motility and which provides a mechanochemical basis for the 'push-pull' theory of locomotion. The model provides a mechanism for how energy stored during lamellipod protrusion can be subsequently used to generate cell body retraction, thus providing a mechanistic link between the MSP assembly dynamics at either end of the cell. In addition to providing a detailed explanation for nematode sperm locomotion, it is likely that many of the concepts explored here are also important in actin-based amoeboid motility. If so, our model could provide a conceptual framework for evaluating many general aspects of cell locomotion.

The authors acknowledge the following support for the research contained herein. G.O. and D.B.: NIH R01 GM59875-01A1. A.M.: NSF DMS-1097749. M.S. and T.R.: NIH GM 29994-19. The work of D.B. was supported also by the NIH postdoctoral fellowship: F32 GM20404-01. D.B. thanks S.B. and many others who have given encouragement and helpful comments as this work progressed.

Appendix

Discussion of the basic physical forces

Protrusion and size regulation

Previously, we demonstrated that actin polymerization in the leading edge of the lamellipod of actin based cells is able to generate both the force to overcome the cell membrane tension and the observed rates of protrusion (Mogilner and Oster, 1996b). The mechanism is the polymerization ratchet: thermal undulations of both filaments and the membrane create a gap between the membrane and the filament tip into which monomers can intercalate. Assembly of monomers onto the polymer tips generates force and unidirectional movement by rectifying Brownian motion. MSP protofilaments appear to be more flexible than actin fibers, suggesting that the polymerization ratchet mechanism may not be sufficient to drive protrusion. However, the process of filament 'bundling' could generate the necessary force and protrusion rates. Here we illustrate this notion using order-of-magnitude estimates.

Consider a protofilament being incorporated into a higher-order MSP fiber at the leading edge that is growing at a rate V_p. This bundling process proceeds by successive adhesion of hydrophobic and electrostatic patches located periodically along the protofilament. Thus, the extension of the bundle results from the binding of the growing, and thermally undulating, tip of the protofilament to other filaments in the bundle. According to the general theory of the polymerization ratchet, this process can generate a force of the order of k_BT/δ, where δ is the distance between the adhesive patches along the protofilaments (Peskin et al., 1993) (A.M. and L. Edelstein-Keshet, unpublished). If $\delta \sim 10$-40 nm, then, one protofilament generates a protrusion force of the order of few tenths of a piconewton. EM images of the leading edge MSP cytoskeleton show that there is roughly one protofilament per 100 nm^2 of the cell's leading edge. Near the stall force, the forces generated by each proto-filament are additive (Van Doorn et al., 2000). The dimensions of the leading edge are ~1 μm×10 μm, so the total protrusion force from the bundling ratchet is $\sim(10\ \mu m^2/0.0001\ \mu m^2)\times 0.1$ pN $\sim 10^4$ pN.

There are no data about the sperm cell membrane tension. Using the scarce data related to some actin-based cells (tens to hundreds of piconewtons per micron of the leading edge), we can estimate the total membrane resistance as 10^2–10^3 pN. Thus, the force of the bundling ratchet would be sufficient to drive protrusion. In the model, we assume that the membrane resistance force is much less than the maximal stall force of the bundling ratchet, and that MSP cytoskeletal growth at the leading edge is load-free.

In addition to the membrane tension, two other factors determine the velocity of protrusion: the intrinsic rate of the bundling ratchet and the free elongation rate of the filaments. The order of magnitude of the former can be estimated as D/δ, where $D \sim 10^7$ nm^2/sec is the effective diffusion coefficient describing thermal writhing of a filament tip δ ~10–40 nm long. The corresponding velocity, $D/\delta \sim 10^3$ μm/sec, clearly cannot be the limiting factor of the observed protrusion rate of ~1 μm/sec. Thus, in the model we assume that the load-free elongation rate of MSP filaments, V_p, is the rate of advancement of the leading edge. Below, we show that the slippage of the cytoskeleton relative to the substratum can be neglected at the leading edge. Therefore, the velocity of lamellipodial advancement is locally normal to the leading edge boundary, and its magnitude is equal to V_p.

Owing to the extremely high concentration of MSP in the sperm cell cytoskeleton (~4 mM), the diffusion of MSP dimers from the rear to the front of the cell is unlikely to limit the rate of assembly. We assume that two factors regulate the net assembly rate. First, polymerization is catalyzed in regions of the leading edge membrane where vesicle protein (VP) and soluble factor (SF) aggregate. The combination of the two correspond to an effective membrane-bound 'enzyme' that catalyzes the activation of MSP monomers from a polymerization-incompetent form into a polymerization-competent configuration. (Either MSP/SF complex can be activated by VP or SF is activated before binding to MSP.) Second, phosphorylation of the VP protein controls its nucleation activity. Another factor controls the location along the margin where this protein is phosphorylated. We use the local pH as the marker for the VP/SF activity and thus assume that V_p is a function of the local pH.

Numerical experiments allowed us to determine the character of the pH dependence of the rate of protrusion. When the assembly rate decreased with pH, as in the 1D model (compare with below), then the sides of the lamellipod gradually collapsed towards the center. On the other hand, if the polymerization rate increased with pH, the lamellipod expanded without limit. If the rate increased at smaller pH values and decreased at greater values, unstable 'mushroom-like' lamellipod shapes ensued. We observed that the following two simple assumptions were sufficient to produce stable lamellipodial size and shape in the simulated cell: (1) cytoskeletal assembly rate increases monotonically with intracellular pH, and (2) there is a depletable factor which limits the size. There are several likely candidates for this additional factor. First, there is evidence for a cytoskeletal component (P25 filament stabilization factor) that dissociates from the fiber complexes just before they are disassembled. If this factor is in limited supply, then an expansion of the lamellipod can lead to its depletion. Second, the vesicle protein itself can be the limiting quantity. If the amount of vesicle protein in the leading edge membrane is constant, then its concentration in the leading edge is diluted as the lamellipodial area increases,

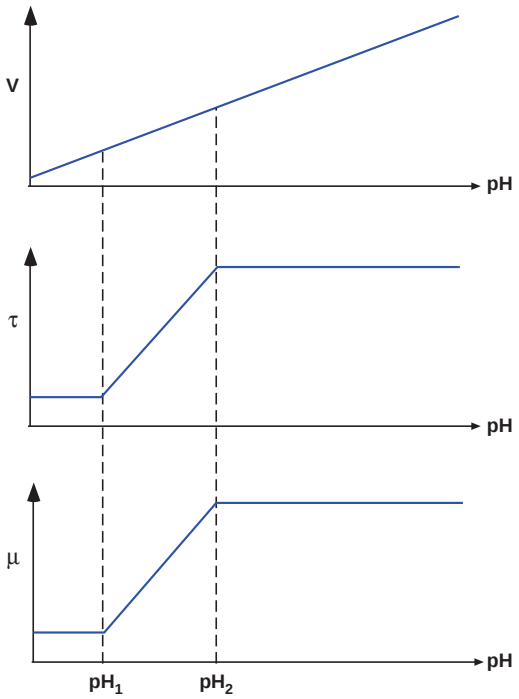

Fig. 6

reducing the MSP polymerization rate. Our simulations show that this is sufficient to regulate the lamellipodial area to a stable average size. The reason for this behavior is that regions of the cell frontier that are closer to the center are at the same time farther from the cell body. Consequently, pH values there are greater, and the protrusion rates are greater. This leads to a stable steady shape of the lamellipod in accordance with the GRE model. Meanwhile, the lamellipodial area cannot grow without limit because of depletion of the limiting factor and slowing down of the leading edge extension.

In the simulations we use the formula:

$$V_p = V_0 \cdot f(pH) \cdot \left(\frac{A_{max} - A}{A_{max}}\right) \qquad \text{(A1)}$$

where V_0=1 μm/sec is the magnitude of the protrusion velocity. The function f(pH) is a linearly increasing function (Fig. 6), such that f(pH=6.05)=0.1, and f(pH=6.15)=1. A is the area of the lamellipod. A_{max} is the area at which the limiting factor controlling the protrusion is completely depleted. In the simulations we used A_{max}=200 μm^2.

Contractile forces

Individual MSP filaments polymerizing near the leading edge membrane are initially stress free and relatively flexible. There is a distribution of filament lengths, but it is not clear what factors determine this distribution. Therefore, we assume an equilibrium configuration characterized by an end-to-end distance, L_0, that is considerably shorter than the fully extended contour length, L. Soon after formation, filaments begin to associate laterally into higher-order filament bundles. Bundling is due to a combination of hydrophobic and electrostatic interactions. The latter arises because, at high pH, the basic groups release their protons and the resulting negative

charges keep the filaments extended beyond their neutral end-to-end length. Thus, newly polymerized MSP filaments find themselves distended beyond their equilibrium length if they were neutral, and hydrophobic bundling locks them into this configuration. This amounts to storing tensile elastic energy that can later be released when the filament unbundle.

We assume that most of the filaments have been extended from their equilibrium length to their contour length: $L_0 \rightarrow L$. A corresponding bundling stress can be estimated as $\tau \sim c\, k_B T((L-L_0)/L_0)$, where c is the volumetric concentration of crosslinks/entanglements. Individual filaments appear to be fairly flexible; there are no direct measures, but we can estimate Lo to be ~10 nm by looking at electron micrographs of negatively stained filaments. The strands (fiber complexes) appear to be very stiff, and the average contour length L can be estimated roughly to be of the order of 100 nm. The reasonable estimate of the average distance between neighboring crosslinks/entanglements is ~30 nm. Then, the parameter c can be estimated as $(1/30\ \text{nm})^3 \sim 3\times10^4\ /\mu m^3$. The strain $((L-L_0)/L_0)$ is of order unity, and the order of magnitude of the bundling stress τ can be estimated as $\tau \sim 100\ \text{pN}/\mu m^2$. In the model, we use the value $\tau_{max}=100\ \text{pN}/\mu m^2$ as the maximal value of the isotropic bundling stress developed at high values of pH.

After formation, the lamellipodial gel remains nearly static (relative to the substratum) because of the high effective friction (see the next section) and the absence of the bundling stress gradient. Eventually, the gel reaches the low pH environment in the perinuclear region. Under the influence of the acidic milieu, the bundling forces weaken. Indeed, the gel is basic so the protonated sites have a low pK_a (i.e. the potential well for proton binding is not too deep: $V/k_BT \approx 2.3 \cdot pK_a$). Therefore, at low proton concentrations the negative binding sites are unoccupied. As the proton concentration increases, the sites become neutralized, thus freeing their counterions to diffuse out of the gel region. This locally lowers the ionic strength, which decreases the difference between the chemical potential of the vapor and the liquid, $(\mu_v - \mu_l)$. According to the current theory of the hydrophobic effect, this weakens the hydrophobic forces between the gel filaments allowing the gel to solate (Lum et al., 1999). Because of the surfactant properties of the liberated counterions, a secondary reinforcing effect is the decrease in surface tension, γ, accompanying the increased ion concentration (Bergethon, 1998). We model these combined effects by lowering the bundling stress from τ_{max} at $pH_2>6.1$ to $\tau_{min}=0.05\ \text{pN}/\mu m^2$ at $pH_1<6.0$. Between pH_1 and pH_2 the bundling stress grows linearly from τ_{min} to τ_{max} (Fig. 6).

In summary, near the cell center, the crosslinking sites protonate, the hydrophobic bundling force weakens and the filament bundles begin to dissociate into their constituent filaments. Each filament that peels off a filament bundle can now shorten to its equilibrium length, L_0; this generates a nearly isotropic contractile stress. Because the substrate adhesive forces are less at the rear of the cell than at the front (see below), this contractile stress pulls the cell body forwards, rather than pulling the cell front rearwards. Thus, bundling of filaments at the cell front and their subsequent unbundling at the cell rear constitutes a 'push-pull' motor that drives the cell forwards. Said another way, bundling creates both the protrusive force at the leading edge and the storage of elastic energy in the lamellipodial gel that is later released to generate the retraction force required to pull up the cell rear.

Graded adhesion

There are two different aspects of adhesion that should be distinguished: the coupling between the MSP cytoskeleton and the cytoplasmic face of the membrane, which is pH sensitive, and the adhesion between the extracellular face of the membrane and the glass coverslip, which may not be pH sensitive. Lowering the extracellular pH disrupts the binding between the cytoskeleton and the membrane, so that the cytoskeleton is pulled back towards the cell body (Italiano et al., 1999). Thus the lamellipod stays extended because the adhesion between cell membrane and the substrate remains intact even though the connection between the cytoskeleton and the membrane is broken. The connection between the cytoskeleton and the substrate is almost certainly mediated through the cell membrane. This could be via transmembrane proteins analogous to integrins or possibly by the MSP attaching to membrane lipids.

In the experimental system, the adhesion appears to be primarily an electrostatic attraction to the glass coverslip that carries a negative surface charge. Although one cannot discount the possibility of transmembrane proteins providing the attachment sites, the ventral surface of the lamellipod can adhere to the substratum even without proteins as follows. Electrostatic interactions should be strongest at the leading edge region where the internal cellular pH is highest. Here the basic MSP gel carries a net positive charge and the inner leaflet of the plasma membrane carries negatively charged lipids. The lipid charges are mobile, whereas the fiber charges are not. Thus, the negative lipids are free to diffuse towards the neighborhood of the fibers, and electrostatic attraction keeps the two in close association. This clustering of negative charge on the inner leaflet induces an opposite clustering of mobile positive charges on the outer membrane leaflet. The proximity of the mobile positively charge membrane with the dense fixed charges of the substratum induces an attractive potential between the two surfaces. The detailed physics of this attractive interaction is discussed in detail in Nardi et al (Nardi et al., 1998), who also show – both theoretically and experimentally – how adhesive 'patches' form that hold the two surfaces together.

The addition of external acetate buffer at $pH_{ext}=6.35$ causes release of cytoskeleton-membrane attachments, but membrane-substratum attachments are retained. The lamellipod remains spread but the cytoskeleton is pulled rearward through the lamellipod. At $pH_{ext}=6.75$, both cytoskeleton-membrane and membrane-substratum attachments are retained. Thus, at the front of the cell where the pH is high, adhesion sites tend to aggregate into larger centers whose adhesions are stronger (Simson and Sackmann, 1998). As the proton concentration increases towards the cell body the adhesion zones shrink and weaken.

We model the adhesion by an effective viscous drag force: if one square micron of the cytoskeleton is dragged at the rate 1 μm/sec, then the effective friction force $f[\text{pN}]=\mu[\text{pN}\times\text{sec}/\mu m^3]\times V[\mu m/\text{sec}]\times 1\ \mu m^2$ is directed against the velocity. To estimate the order of magnitude of the effective drag coefficient, μ, we use the effective energy of the strong adhesion of the unit area of the cell to the substratum, $W\sim1\ \text{pN}/\mu m$ (Nardi et al., 1998). Let us assume that this adhesion is due to effective dynamic crosslinks between the membrane and the cytoskeleton, which act as effective Hookean springs. We assume that the springs break when they are extended beyond a distance $\delta\sim10$ nm (a characteristic length for

conformation change of many cytoskeletal proteins). Then, the characteristic force associated with pulling the cytoskeleton off the surface is $W/\delta \sim 100$ pN/μm^2. We will assume that when the rate of the cytoskeletal flow is V_0=1 μm/sec, then the effective friction is associated with breaking the crosslinks. This would imply that at this velocity and higher, the friction is velocity independent and nearly constant. However, we will also assume that at lower velocities the friction is due to spontaneous dissociation of the effective crosslinking springs stretched below their yield. In this situation the friction force at lower velocities can be approximated by an effective viscous drag force, where the corresponding coefficient μ has the form: $\mu \sim (W/\delta V_0) \sim 100$ pN×sec/μm^3 (Leibler and Huse, 1993). In the model, we use the following dependence of the parameter μ on pH (Fig. 6): at pH_2>6.1, μ_{max}=100 pN×sec/μm^3, while at pH_1<6.0, μ_{min}=5 pN×sec/μm^3. Between pH_1 and pH_2 the viscous drag coefficient grows linearly from μ_{min} to μ_{max}.

Note that in the model we neglected the effective resistance associated with relative motion of the cytoskeleton and the aqueous phase of the cytoplasm. Its order of magnitude can be as high as that from the adhesion between the cytoskeleton and the membrane: ~100 pN×sec/μm^4×1 μm, where 1 μm is the height of the lamellipod and 100 pN×sec/μm^4 is the order of magnitude of the dense gel drag coefficient (Tanaka and Fillmore, 1979). This is an overestimate because it assumes that the fluid is stationary, whereas in fact it partially follows the gel movement. An accurate treatment of these effects requires a two-phase model; this will be reported in a subsequent publication (C. Wolgemuth et al., unpublished).

We model the cell body as a rigid domain (see below) characterized by the drag coefficient $\mu_{cb}=10^3$ pN×sec/μm^3. We will demonstrate that the total area of the lamellipod is ~100 μm^2. Thus, the total drag coefficient of the lamellipod is ~100 pN×sec/μm^3×100 μm^2 =10^4 pN×sec/μm>>μ_{cb}. We will see that the area of the contracting part of the lamellipod at the rear has an area ~10 μm^2. The net contractile force can be estimated as 100 pN/μm^2×10 μm^2 =10^3 pN. This force pulls the cell body forward at the rate ~10^3 pN/10^3 pN×sec/μm^3=1 μm/sec. At the same time, the rate of retrograde flow (relative to the substratum) is much smaller ~10^3 pN/10^4 pN×sec/μm ~ 0.1 μm/sec.

Continuous model equations

The lamellipodial domain is denoted by Ω, defined by the union of two boundaries: the leading edge boundary, where the MSP cytoskeleton is assembled, $\partial\Omega_F$, and the cell body interface, $\partial\Omega_R$. The model consists of four sub-models: protrusion, contraction, adhesion and pH distribution. The first three govern the essential mechanics of locomotion, and the last is the biochemical mechanism synchronizing the motility mechanics. Together, they constitute a minimal mechanochemical locomotory machine.

pH distribution

We model the proton distribution on the 2D lamellipodial domain, Ω, by the reaction-diffusion equation:

$$\frac{\partial [H^+]}{\partial t} = \underbrace{D\nabla^2[H^+]}_{\text{Diffusion}} - \underbrace{P\left([H^+]-[H^+]_{ext}\right)}_{\text{Leakage}} \qquad \text{(A2)}$$

The reaction term is responsible for proton leakage across the cell membrane; the flux is proportional to the local difference between the lamellipodial and extracellular proton concentrations. P is the corresponding permeability of the cell membrane. The boundary conditions are given by:

$$\nabla[H^+]\cdot\mathbf{n} = \begin{cases} h_B\Phi & \text{cell body interface} \\ h_L P\left([H^+]-[H^+]_{ext}\right) & \text{lamellipodial boundary} \end{cases} \qquad \text{(A3)}$$

Here Φ is the proton influx from the cell body, h_L is the thickness of the lamellipod in the vertical direction, h_B is the thickness of the cell body interface in the vertical direction, and n is the local unit vector normal to the boundary. The diffusion of protons is very fast, and the proton concentration relaxes to its steady state very fast relative to the time scale of cell motion. The latter is ~10 seconds and can be estimated as the characteristic size of the lamellipod, 10 μm, divided by the characteristic rate of motion, 1 μm/sec. Thus the temporal dynamics of the proton distribution can be scaled out, and the proton distribution can be described by the Helmholtz equation:

$$\nabla^2[H^+] - p\left([H^+]-[H^+]_{ext}\right) = 0 \qquad \text{(A4)}$$

where p=P/D, along with the boundary conditions (A3). Equations (A3) and (A4) are solved on the current lamellipodial domain at each computational time step and the pH distribution calculated as

$$pH = -\log_{10}([H^+]) \qquad \text{(A5)}$$

For a lamellipodial size ~10 μm×10 μm and pH_{ext}=7.6, the pH at the base of the lamellipod is ≈5.95, and the pH increases by ≈0.2 units from the rear to the front of the lamellipod. We have chosen the model parameters (Φ, h_L, h_B, p) to conform to these observations.

Protrusion

We model protrusion by moving the leading edge boundary locally in the direction normal to the boundary at the rate given by formula (A1) . The pH dependence of the protrusion is shown in Figure 6. Both pH and lamellipodial area in (A1) are computed at each point of the leading edge boundary at each computational time step.

Contraction

The mechanics of the 2D lamellipod are approximated by the linear elasticity equation for the displacement:

$$\underbrace{\mu(\mathbf{x})\frac{\partial \mathbf{u}}{\partial t}}_{\substack{\text{Substratum}\\ \text{drag}}} = \underbrace{\left(\frac{Y}{2(1+\nu)}\right)\nabla^2\mathbf{u} + \left(\frac{Y}{2(1+\nu)(1-2\nu)}\right)\nabla(\nabla\cdot(\mathbf{u}))}_{\text{Gel elasticity}} - \underbrace{\nabla\tau(pH(\mathbf{x}))}_{\substack{\text{Bundling}\\ \text{stress}}}, \qquad \text{(A6)}$$

where u(x, t) is the small displacement of the cytoskeletal material point during each time step, such that at the time when the point was created at the leading edge boundary the displacement is zero. Y is Young's modulus and ν is the Poisson ratio. The left-hand side of equation (A6) describes the body-force associated with breaking the adhesion bonds between the cytoskeleton and the surface. The first two terms on the right hand side are responsible for the elastic deformation forces in the cytoskeleton. The last term describes the force created by the gradient of the isotropic bundling stress, which is a function of the local pH described in 'Forces

in the lamellipod' (Fig. 6). The Poisson ratio of the cytoskeletal gel is ~1. The Young's modulus can be estimated using the formula from the theory of rubber elasticity (Doi and Edwards, 1986; Tanaka and Fillmore, 1979): $Y \sim nk_BT$, where n is the concentration of fiber strands between crosslinks/entanglements in the cytoskeleton. Assuming that the average distance between the crosslinks is ~30 nm, $n \sim 2.5\times 10^4/\mu m^3$ and $Y \sim 100$ pN/μm^2. In the 2D model, Y has dimension [pN/μm] and can be obtained from the 3D Young's modulus by multiplying the 3D modulus by the height of the lamellipod, ~1 μm. In the model, we use the value Y=100 pN/μm. Equation (A6) must be complemented by the boundary conditions of zero displacement at the leading edge boundary and given total stress at the cell body interface:

$$\begin{aligned} &\mathbf{u}(\mathbf{x}) = 0\,, && \mathbf{x} \in \partial\Omega_F\,, \\ &\sigma(\mathbf{x})\cdot\mathbf{n}(\mathbf{x}) = F_I(\mathbf{x})\,, && \mathbf{x} \in \partial\Omega_R \\ &\mu(\mathbf{x}) = \mu(pH(\mathbf{x})) \end{aligned} \qquad \text{(A7)}$$

The first condition assumes no slippage of the cytoskeleton at the leading edge, a very good assumption according to experimental observations. In the second condition, the force F_I at the interface between the lamellipod and the cell body depends on the nature of the connection between the cell body and the cytoskeleton and on the dynamics of the depolymerization process at the rear of the lamellipod. Neither of these factors is yet known. Mathematically, the most general boundary conditions at the cell body interface are local dynamic depolymerization equations complemented with force-velocity conditions. Derivation of the latter requires detailed understanding of the coupling between the cytoskeleton and the cell body. In the model, we assume that a constant force of magnitude F_I=1000 pN/μm is developed at the cell body interface. This assumes that most of the bundling stress is used to develop the force pulling the cell body forward. This assumption corresponds, for example, to the following (rather artificial) process of MSP cytoskeleton disassembly. At the rear, most bundles are disassembled, and the cytoskeleton consists of the rubber-like strands. Consider the strands attached at one end to another cytoskeletal strand and at the other end to the cell body boundary. Only these strands generate the force at the cell body interface. Then, impose the following 'stress-dependent depolymerization' relation: the strands stretched below a certain threshold are depolymerized instantly, the rest of the strands are not depolymerized. Then, the stress at the cell body interface is always slightly above this threshold. At the same time, this condition prevents an unbounded increase in concentration of the cytoskeleton at the lamellipodial base as the cell moves forward.

Adhesion

The effective drag coefficient, μ, used in equation (A6) is the function of pH given in above (Fig. 6).

Equations (A2)-(A7) constitute a self-consistent mechanochemical model of the MSP cytoskeleton on a free boundary domain. In the next section we solve the 1D version of these equations. Then, we explain the 2D finite element model based on the continuous model introduced here.

Steady motion of a 1D gel strip

Consider the 1D cytoskeletal strip of length L(t)=f(t)-r(t), where f(t) is the coordinate of the front (leading edge) of the lamellipod, and r(t) is the coordinate of the rear (cell body) interface. The 1D Helmholtz equation for the proton concentration $h \equiv [H^+]$ has the simple form:

$$\frac{d^2h}{dx^2} - p\cdot h = 0\,, \qquad \text{(A8)}$$

with solution

$$h \approx h_r \exp[-\sqrt{p}(x-r)] \qquad \text{(A9)}$$

Thus, the pH increases linearly with the distance from the rear:

$$pH(x) = pH_r + \alpha(x-r)\,, \qquad \alpha = \text{const.} \qquad \text{(A10)}$$

Both the adhesion gradient and bundling stress are reflected in the pH-dependent functions, μ(pH(x)) and τ(pH(x)), respectively. Let L_c be the distance from the rear, such that $pH(L_c) = pH_1$, and L_c' the distance at which $pH(L_c') = pH_2$ (Fig. 6). We will assume for simplicity that $(L_c'-L_c) \ll L_c$, so the drag coefficient and the bundling stress can be approximated by the step functions:

$$(\mu,\tau)(x) = \begin{cases} (\mu,\tau)_{min} & r \le x \le r + L_c \\ (\mu,\tau)_{max} & r + L_c < x \le f \end{cases} \qquad \text{(A11)}$$

On the interior of the domain, x = [r(t), f(t)], the stress is

$$\sigma = Y\frac{\partial u}{\partial x} - \tau(x) \qquad \text{(A12)}$$

and the equation of motion has the form:

$$\mu(x)\frac{\partial u}{\partial t} = \frac{\partial \sigma}{\partial x} = Y\frac{\partial^2 u}{\partial x^2} - \frac{\partial \tau}{\partial x} = Y\frac{\partial^2 u}{\partial x^2} - \Delta\tau\cdot\delta(x - r(t) - L_c)\,, \qquad \text{(A13)}$$

where $\Delta\tau = \tau_{max} \equiv \tau_{min}$, and $\delta(\cdot)$ is the Dirac delta-function.

We seek the solution corresponding to the steady movement of the 1D strip with a constant length, L, and a constant speed, V:

$$r = r(x - Vt), \quad f = r + L\,, \qquad (\mu,\tau) = (\mu,\tau)(x - Vt) \qquad \text{(A14)}$$

Introduce the traveling-wave coordinate z = x – Vt, so that z = 0, L corresponds to x = r(t), f(t), respectively. Then, the equation of motion becomes the ordinary differential equation:

$$-\mu(z)V\frac{du}{dz} = Y\frac{d^2u}{dz^2} - \Delta\tau\cdot\delta(z - L_c)\,, \quad \mu(z) = \begin{cases} \mu_{min} & 0 \le z \le L_c \\ \mu_{max} & L_c < x \le L \end{cases} \qquad \text{(A15)}$$

It is convenient to introduce the strain, ε = du/dz, and rewrite the equation of motion for the strain:

$$\frac{d\varepsilon}{dz} + \frac{\varepsilon}{l(z)} = \frac{\Delta\tau\cdot\delta(z - L_c)}{Y}\,, \qquad l(z) = \frac{Y}{V}\cdot\begin{cases} 1/\mu_{min} & 0 \le z \le L_c \\ 1/\mu_{max} & L_c < z \le L \end{cases} \qquad \text{(A16)}$$

The equation for the strain can be solved explicitly in closed form using the boundary condition for the stress at the rear:

$$Y\varepsilon(0) - \tau(0) = F\,, \qquad \varepsilon(0) = \frac{1}{Y}(F + \tau_{min}) \qquad \text{(A17)}$$

where F is the force at the cell body interface. The solution has the form:

$$\varepsilon(z)=\begin{cases}\dfrac{F+\tau_{min}}{Y}\exp[-z/l_1] & l_1=\dfrac{Y}{V\mu_{min}},\quad 0\le z\le L_c\\ \left(\dfrac{F+\tau_{min}}{Y}\exp[-L_c/l_1]+\dfrac{\Delta\tau}{Y}\right)\exp[-(z-L_c)/l_2] & l_2=\dfrac{Y}{V\mu_{max}},\quad L_c<z\le L\end{cases} \tag{A18}$$

This strain distribution is shown in Fig. 7 for the model parameters Y, F, τ_{min}, τ_{max}, μ_{min}, μ_{max} given above, and L_c= 1 μm and V=1 μm/sec.

The rate of retrograde flow (relative to the substratum) is equal to $-V\varepsilon(z)$. Thus, Fig. 7 demonstrates that there is virtually no slippage of the cytoskeleton in the front half of the lamellipod. This is due to the strong inequality $Y<<\mu_{max}$ V: adhesion at the front is strong enough to prevent slipping. This result validates the boundary condition u(L)=0 at the front. The strain builds up sharply in front of the interface with the contractile zone. Both strain and retrograde flow reach maxima at the contractile interface where the bundling stress drops, elastic energy is released to pull the lamellipod backward and the cell body forward.

The velocity of forward translocation of the cell body, V, can be found balancing the contraction force at the rear of the lamellipod, F, with the frictional drag force on the cell body:

$$F=\mu_{c.b.}V,\qquad V=\frac{F}{\mu_{c.b.}} \tag{A19}$$

Finally, the equilibrium length of the lamellipod can be obtained from the condition that the velocity of the cell body is equal to the rate of leading edge extension, $V_p(L)$, minus the slip velocity, $V\varepsilon(L)$, neglecting the exponentially small slippage, $V_p(L)\approx V$. Using equation (A1), where the lamellipodial length is substituted for the area, and the fact that pH increases linearly with the distance from the rear, we obtain

$$V_0(1+\tilde{\alpha}L)\frac{L_{max}-L}{L_{max}}=\frac{F}{\mu_{c.b.}} \tag{A20}$$

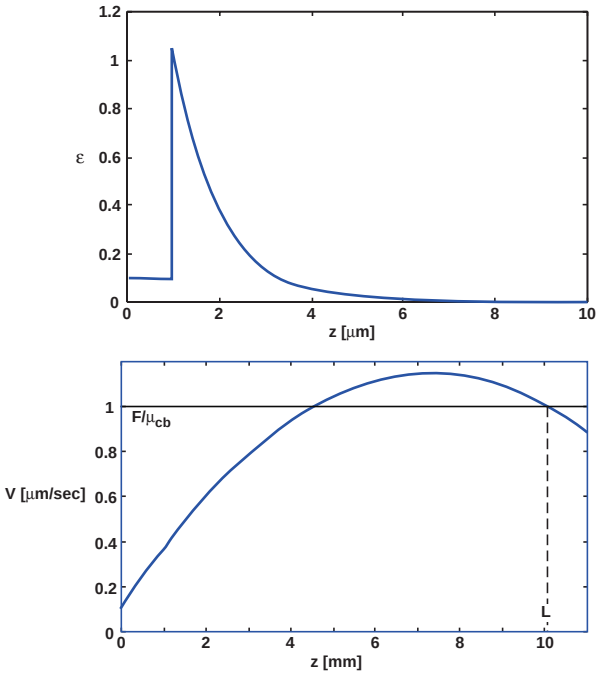

Fig. 7

a quadratic equation for the lamellipodial length, L. Note, that in our model the rate of forward translocation is determined by the conditions at the rear of the lamellipod, providing that the bundling stress is built in at the front. Then the length of the lamellipod adjusts so that its protrusion rate matches the rate of the cell body translocation. For the values of the model parameters, equation (A20) has two solutions (Fig. 8). The smaller value of L is unstable but the larger value (~10 μm) is stable.

The numerical simulation method

Rather than solving the partial differential equations on the 2D free boundary domain formulated above, we construct a finite element model having all essential qualitative and quantitative features of the continuous model. The shape of the cell body domain is fixed, as in the continuous model, and its motion is associated with an effective viscous friction described above. We model the cell-body interface (CBI) by ~15 permanent nodes. The 2D interior (I) of the lamellipodial cytoskeleton is modeled by ~60 interior nodes that are dynamic: they move, appear and disappear according to the rules described below. LE of the lamellipod is modeled by ~25 nodes at the free boundary of the lamellipod. An unstructured grid is natural for the description of the moving viscoelastic cytoskeleton. Each node represents the MSP cytoskeleton within the corresponding territory consisting of the points closer to this given node than to any other node. Such cells are called Voronoi polygons, or Voronoi tiles (Okabe, 2000). The neighboring nodes are connected by edges that are normal to the corresponding faces of the Voronoi tiles. Together, the nodes and edges triangulate the lamellipod by a set of dynamic 'Delaunay triangles' that represent the lamellipodial domain.

Denote by l_{ij} the distance between the i^{th} and j^{th} nodes (i.e. the length of the corresponding Delaunay edge) and by v_{ij} the length of the Voronoi face (Fig. 8). Let A_i be the area of the Voronoi tile surrounding the i^{th} node. The four submodels of the continuous mechanochemical model have the following discrete analogues.

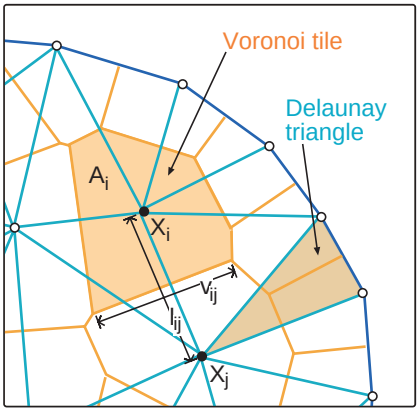

Fig. 8

pH distribution

We describe the proton concentration as a function defined on the set of nodes. The discretized Helmholtz equation has the form:

$$\frac{1}{A_i}\sum_j \frac{[H^+]_i-[H^+]_j}{l_{ij}}v_{ij}-p\left([H^+]_i-[H^+]_{ext}\right)=0 \qquad \text{(A21)}$$

The pH distribution is characterized by the values at the nodes and at the edges connecting the nodes:

$$\underset{\text{Node i}}{pH_i}=-\log_{10}([H^+]_i),\qquad \underset{\text{Edge between node i and j}}{pH_{ij}}=-\log_{10}\left(\frac{1}{2}([H^+]_i+[H^+]_j)\right) \qquad \text{(A22)}$$

Dynamic graded adhesion

A sliding friction element between the cell and the substratum is associated with each node. The corresponding drag coefficient for the i^{th} I nodes is given by the function introduced above: $\mu_i=\mu(X_i)=\mu(pH_i)$. The CBI nodes are not assigned sliding friction elements; rather the resistance of the cell body to movement is associated with a single composite drag coefficient, μ_{cb}. The LE nodes are associated with the villipodial protrusions, which do not adhere to the substratum. Thus, each LE node has a very weak sliding friction element characterized by the effective drag coefficient $\mu_i=\mu_0<<\mu_{min}$ (the effective drag coefficient for the boundary nodes is due to the drag experienced by the leading edge moving through the ambient fluid).

Contraction and protrusion

Associated with each Delaunay edge connecting neighboring nodes is a Hookean spring with zero rest length and a tensile element. The spring is responsible for the elastic stress in the cytoskeleton and the tensile element for the bundling stress associated with the edge connecting the i^{th} and j^{th} nodes. The bundling stress is specified by the function $\tau(pH)$ defined in Section 0: $F_{ij}^{bundl}=\tau(pH_{ij})$. The elastic force density between these nodes is $F_{ij}^{elast}=\kappa\cdot l_{ij}$. The constant $\kappa\sim YP_1/\langle l_{ij}\rangle\sim 100$ pN/μm^2, where Y=100 pN/μm^2 is the 3D Young's modulus, $h_1\sim 1$ μm is the height of the lamellipod, and $\langle l_{ij}\rangle\sim 1$ μm is the average distance between the nodes.

The force applied to all I and CBI nodes is given by the equation

$$f_i=\sum_j (F_{ij}^{elast}-F_{ij}^{bundl})v_{ij}\frac{X_j-X_i}{|X_j-X_i|},\qquad F_{ij}^{elast}=\kappa\cdot l_{ij} \qquad \text{(A23)}$$

where the summation goes over all nodes connected to the given one by a Delaunay edge.

Protrusion is modeled by adding the rest length, l_{ij}^{rest}, to each of the Delaunay edges connecting pairs of nodes, such that one of them is an I node and another is an LE node. The rest length is a function of time such that the rate of increase of the rest length is equal to the local protrusion rate:

$$\Delta l_{ij}^{rest}=V_{ij}\Delta t, V_{ij}=V_0 f(pH_{ij})\frac{\left(A_{max}-A_{lamel}\right)}{A_{max}},\quad A_{lamel}=\sum_i A_i \qquad \text{(A24)}$$

where Δt is the integration time step, and the dependence of the protrusion rate on pH and area was explained above. The force applied to all LE nodes is given by the equation

$$f_i=\sum_j (F_{ij}^{elast}-F_{ij}^{bundl})v_{ij}\frac{X_j-X_i}{|X_j-X_i|}+\kappa_m\left(\frac{X_{i+1}-X_i}{|X_{i+1}-X_i|}+\frac{X_{i-1}-X_i}{|X_{i-1}-X_i|}\right),\ F_{ij}^{elast}=\kappa(l_{ij}-l_{ij}^{rest}) \qquad \text{(A25)}$$

Here the additional term $\kappa_m(X_{i+1}+X_{i-1}-2X_i)$ models the membrane tension. The effective spring constant κ_m=10 pN/μm corresponds to our estimates of the membrane resistance at the beginning of the Appendix.

Equations of motion

From the above formulas the equations of motion can be assembled as follows.

CBI nodes

The force, f_i, applied to each CBI node is computed according to equation (A23). The total force and torque applied to the rigid cell body are computed as the geometric sum of the cytoskeletal forces and torques applied to all CBI nodes. The corresponding translocation velocity of the center-of-mass and the angular velocity of the cell body is computed and is moved over the computational step Δt accordingly.

I and LE nodes

The forces f_i applied to each I and LE node are computed according to formulae (A23), (A24) and (A25). Then, each node is moved according to the equation

$$\Delta X_i=\Delta t\left(\frac{f_i}{\mu_i A_i}\right) \qquad \text{(A26)}$$

analogous to the continuous equation of motion (A6).

Assembly, disassembly and remodeling of the cytoskeleton

Insertion of new nodes

If $l_{ij}=|X_i-X_j|$ becomes longer than an upper threshold length ($l_{ij}<l_{max}$), then a new node is inserted between the i^{th} and j^{th} nodes at $(X_i-X_j)/2$. Although the algorithm does not explicitly preclude the insertion of nodes anywhere in the lamellipod, in the actual simulations, the net gain of nodes takes place only near the leading edge of the moving cell. The former models the polymerization process. Without the latter, the lateral flow would deplete the cytoskeleton at the leading edge. In the computations, we use the value l_{max}=3 μm.

Deletion of nodes

The i^{th} node is deleted if $l_{ij}=|X_i-X_j|$ becomes shorter than a lower threshold ($l_{ij}<l_{min}$) and the j^{th} node is a CBI node. This process models the disassembly and the unbundling at the rear of the lamellipod. In the computations, we use the value l_{min}=0.7 μm. This corresponds to the observed width of the depolarization zone at the rear of the lamellipod ~1 μm. This

corresponds to the assumption that the rubber-like strands attached to the cell body depolymerize when their strain becomes less than a lower threshold. This algorithm generates an average force of ~1000 pN applied to the cell body.

Simulations

The model parameters are given here and at the beginning of the Appendix. We non-dimensionalize the equations of the model using a length scale of 2 μm and a time scale of 2 μm/(1 μm/sec)=2 seconds. We solved equations (A21)-(A26) using a time step equal to one hundredth of the time scale. The computations were performed using MATLAB™ (v5.3r11). The simulation requires approximately 30 minutes execution time on a P2 450 Mhz processor for the model cell to translocate by one body length. After a brief transient, the cell moves persistently with a constant shape and velocity.

References

Abercrombie, M. (1980). The Croonian lecture, 1978. The crawling movement of metazoan cells. *Proc. Roy. Soc. Lond. B* **207**, 129-147.

Bergethon, P. R. (1998). The Physical Basis Of Biochemistry: The Foundations Of Molecular Biophysics. New York: Springer.

Blanchoin, L., Pollard, T. and Mullins, R. (2000). Interactions of ADF/cofilin, Arp2/3 complex, capping protein and profilin in remodeling of branched actin filament networks. *Curr. Biol.* **10**, 1273-1282.

Borisy, G. and Svitkina, T. (2000). Actin machinery: pushing the envelope. *Curr. Opin. Cell Biol.* **12**, 104-112.

Bottino, D. (2001). Computer simulations of mechanochemical coupling in a deforming domain: Applications to cell motion. In *IMA Frontiers in Applications of Mathematics: Mathematical Models for Biological Pattern Formation*, pp. 295. New York: Springer.

Bullock, T., McCoy, A., Kent, H., Roberts, T. and Stewart, M. (1998). Structural basis for amoeboid motility in nematode sperm. *Nat. Struct. Biol.* **5**, 184-189.

Bullock, T., Roberts, T. and Stewart, M. (1996). 2.5 Å resolution crystal structure of the motile major sperm protein (MSP) of *suum*. *J. Mol. Biol.* **263**, 284-296.

Cameron, L., Footer, M., Oudenaarden, A. and Theriot, J. (1999). Motility of ActA protein-coated microspheres driven by actin polymerization. *Proc. Natl. Acad. Sci. USA* **96**, 4908-4913.

Dembo, M., Oliver, T., Ishihara, A. and Jacobson, K. (1996). Imaging the traction stresses exerted by locomoting cells with the elastic substratum method. *Biophys. J.* **70**, 2008-2022.

Doi, M. and Edwards, S. (1986). The Theory of Polymer Dynamics. New York: Oxford University Press.

Ellis, R. (2001). Macromolecular crowding: an important but neglected aspect of the intracellular environment. *Curr. Opin. Struct. Biol.* **11**, 114-119.

Italiano, J., Roberts, T., Stewart, M. and Fontana, C. (1996). Reconstitution in vitro of the motile apparatus from the amoeboid sperm of ascaris shows that filament assembly and bundling move membranes. *Cell* **84**, 105-114.

Italiano, J., Stewart, M. and Roberts, T. (1999). Localized depolymerization of the major sperm protein cytoskeleton correlates with the forward movement of the cell body in the amoeboid movement of nematode sperm. *J. Cell Biol.* **146**, 1087-1095.

Italiano, J., Stewart, M. and Roberts, T. (2001). How the assembly dynamics of the nematode major sperm protein generate amoeboid cell motility. *Int. Rev. Cytol.* **202**, 1-34.

Jacobson, K., Oliver, T., Dembo, M., Ishihara, A., Yang, B., Navarrer, R. and Lee, J. (1996). Imaging the traction forces exerted by locomoting keratocytes. *Prog. Biophys. Mol. Biol.* **65**, 17.

King, K., Stewart, M., Roberts, T. and Seavy, M. (1992). Structure and macromolecular assembly of two isoforms of the major sperm protein (MSP) from the amoeboid sperm of the nematode, *suum*. *J. Cell Sci.* **101**, 847-857.

King, K., Essig, J., Roberts, T. and Moerland, T. (1994a). Regulation of the major sperm protein (MSP) cytoskeleton by intracellular pH. *Cell Motil. Cytoskeleton* **27**, 193-205.

King, K., Stewart, M. and Roberts, T. (1994b). Supramolecular assemblies of the suum major sperm protein (MSP) associated with amoeboid cell motility. *J. Cell Sci.* **107**, 2941-2949.

Knecht, D. and Loomis, W. (1987). Antisense RNA inactivation of myosin heavy chain gene expression in Dictyostelium discoideum. *Science* **236**, 1081-1085.

Landau, L. and Lifshitz, E. (1995). The Theory of Elasticity. Boston: Butterworth-Heinemann.

Lee, J., Ishihara, A. and Jacobson, K. (1993a). The fish epidermal keratocyte as a model system for the study of cell locomotion. In *Cell Behaviour: Adhesion and Motility*, vol. 47 (eds G. Jones C. Wigley and R. Warn), pp. 73-90. Cambridge: The Company of Biologists, Ltd.

Lee, J., Ishihara, A., Theriot, J. A. and Jacobson, K. (1993b). Principles of locomotion for simple-shaped cells. *Nature* **362**, 467-471.

Leibler, S. and Huse, D. (1993). Porters versus rowers: a unified stochastic model of motor proteins. *J. Cell Biol.* **121**, 1357-1368.

Lin, C., Espreafico, E., Mooseker, M. and Forscher, P. (1996). Myosin drives retrograde F-actin flow in neuronal growth cones. *Neuron* **16**, 769-782.

Lum, K., Chandler, D. and Weeks, J. (1999). Hydrophobicity at small and large length scales. *J. Phys. Chem. B* **103**, 4570-4577.

Manning, G. and Ray, J. (1998). Counterion condensation revisited. *J. Biomol. Struc. Dynam.* **16**, 461-476.

Miller, M., Nguyen, V., Lee, M., Kosinski, M., Schedl, T., Caprioli, R. and Greenstein, D. (2001). A sperm cytoskeletal protein that signals oocyte meiotic maturation and ovulation. *Science* **291**, 2144-2147.

Mogilner, A. and Oster, G. (1996a). Cell motility driven by actin polymerization. *Biophys. J.* **71**, 3030-3045.

Mogilner, A. and Oster, G. (1996b). The physics of lamellipodial protrusion. *Eur. Biophys. J.* **25**, 47-53.

Nardi, J., Bruinsma, R. and Sackmann, E. (1998). Adhesion-induced reorganization of charged fluid membranes. *Physical Review E* **58**, 6340-6354.

Okabe, A. (2000). Spatial tessellations: concepts and applications of Voronoi diagrams. Chichester; New York: Wiley.

Oliver, T., Dembo, M. and Jacobson, K. (1995). Traction forces in locomoting cells. *Cell Motil. Cytoskeleton* **31**, 225-240.

Oliver, T., Dembo, M. and Jacobson, K. (1999). Separation of propulsive and adhesive traction stresses in locomoting keratocytes. *J. Cell Biol.* **145**, 589-604.

Oster, G. (1988). Biophysics of the leading lamella. *Cell Motil. Cytoskeleton* **10**, 164-171.

Oster, G. and Perelson, A. (1988). The physics of cell motility. In *Cell Behavior: Shape, Adhesion and Motility*, vol. 8 (ed. C. M. J. Heaysman, F. Watt), pp. 35-54. Cambridge, England: The Company of Biologists Ltd.

Pantaloni, D., Le Clainche, C. and Carlier, M.-F. (2001). Mechanism of actin-based motility. *Science* **292**, 1502-1506.

Peskin, C. S., Odell, G. M. and Oster, G. (1993). Cellular motions and thermal fluctuations: the Brownian ratchet. *Biophys. J.* **65**, 316-324.

Pollack, G. (2001). Cells, Gels and the Engines of Life. Seattle, WA: Ebner & Sons.

Pollard, T., Blanchoin, L. and Mullins, R. (2000). Molecular mechanisms controlling actin filament dynamics in nonmuscle cells. *Annu. Rev. Biophys. Biomol. Struct.* **29**, 545-576.

Pollard, T. D., Blanchoin, L. and Mullins, R. D. (2001). Actin dynamics. *J. Cell Sci.* **114**, 3-4.

Raucher, D. and Sheetz, M. (1999a). Characteristics of a membrane reservoir buffering membrane tension. *Biophys. J.* **77**, 1992-2002.

Raucher, D. and Sheetz, M. (1999b). Membrane expansion increases endocytosis rate during mitosis. *J. Cell Biol.* **144**, 497-506.

Raucher, D. and Sheetz, M. (2000). Cell spreading and lamellipodial extension rate Is regulated by membrane tension. *J. Cell Biol.* **148**, 127–136.

Roberts, T. and Stewart, M. (1995). Nematode sperm locomotion. *Curr. Opin. Cell Biol.* **7**, 13-17.

Roberts, T. and Stewart, M. (1997). Nematode sperm: Amoeboid movement without actin. *Trends Cell Biol.* **7**, 368-373.

Roberts, T. and Stewart, M. (2000). Acting like actin: The dynamics of the nematode major sperm protein (MSP) cytoskeleton indicate a push-pull mechanism for amoeboid cell motility. *J. Cell Biol.* **149**, 7-12.

Roberts, T., Salmon, E. and Stewart, M. (1998). Hydrostatic pressure shows that lamellipodial motility in sperm requires membrane-associated major sperm protein filament nucleation and elongation. *J. Cell Biol.* **140**, 367-375.

Royal, D., Royal, M., Italiano, J., Roberts, T. and Soll, D. (1995). In sperm pseudopods, MSP fibers move proximally at a constant rate regardless of the forward rate of cellular translocation. *Cell Motil. Cytoskeleton* **31**, 241-253.

Sepsenwol, S. and Taft, S. J. (1990). In vitro induction of crawling in the amoeboid sperm of the nematode parasite, Ascaris *suum*. *Cell Motil. Cytoskeleton* **15**, 99-110.

Sepsenwol, S., Ris, H. and Roberts, T. (1989). A unique cytoskeleton associated with crawling in the amoeboid sperm of the nematode, *suum*. *J. Cell Biol.* **108**, 55-66.

Simson, R. and Sackmann, E. (1998). Mimicking physics of cell adhesion. In *Summer School 1998*. Simon Fraser University.

Stevens, M. (1999). Bundle binding in polyelectrolyte solutions. *Phys. Rev. Lett.* **82**, 101-104.

Stevens, M. (2001). Simple simulations of DNA condensation. *Biophys. J.* **80**, 130–139.

Stewart, M., King, K. and Roberts, T. (1994). The motile major sperm protein (MSP) of *suum* forms filaments constructed from two helical subfilaments. *J. Mol. Biol.* **243**, 60-71.

Strang, G. (1986). Introduction to Applied Mathematics. Wellesley, Mass.: Wellesley-Cambridge Press.

Svitkina, T., Verkhovsky, A., McQuade, K. and Borisy, G. (1997). Analysis of the actin-myosin II system in fish epidermal Keratocytes: Mechanism of cell body translocaction. *J. Cell Biol.* **139**, 397-415.

Tanaka, T. and Fillmore, D. (1979). Kinetics of swelling of gels. *J. Chem. Phys* **70**, 1214-1218.

Taylor, D., Hellewell, S., Virgin, H. and Heiple, J. (1979). The solation-contraction coupling hypothesis of cell movements. In: Cell Motility: Molecules & Organization p. 363-77. Tokyo: University of Tokyo Press.

Theriot, J. (2000). The polymerization motor. *Traffic* **1**, 19–28.

Van Doorn, G., Tanase, C., Mulder, B. and Dogterom, M. (2000). On the stall force for growing microtubules. *Eur. Biophys. J.* **29**, 2-6.

Verkhovsky, A., Svitkina and Borisy, G. (1999). Self-polarization and directional motility of cytoplasm. *Curr. Biol.* **9**, 11-20.

Verkhovsky, A. B., Svitkina, T. M. and Borisy, G. G. (1995). Myosin II Filament assemblies in the active lamella of fibroblasts: their morphogensis and role in the formation of actin filament bundles. *J. Cell Biol.* **131**, 989-1002.